Detection of Biofilm Forming Microbes Using Electrochemical Methods
by

Yongxu Chen

A thesis submitted in partial fulfillment of the requirements for the degree of

Master of Science

Department of Renewable Resources
University of Alberta

ABSTRACT

Microbiologically Influenced Corrosion (MIC) and biofouling are major challenges to operators who manage water systems in the oil & gas and other sectors. The root caused for these threats is the formation and accumulation of biofilms in piping systems due to the agglomeration of both biotic components (e.g. bacteria, archaea and extracellular polymeric substances) and abiotic materials (e.g. inorganic solids). These biofilms adhere to inner pipe wall surfaces and evolve over time, depending on surrounding environmental conditions, eventually lead to corrosion.

In this study, a novel in-situ method to detect the presence of biofilm-forming bacteria in a fluid system has been proposed based on capacitance measurements using the Electrochemical Impedance Spectroscopy (EIS) technique. Two probe types were assessed to detect and measure the growth of bacteria: 1) a parallel plate system, and 2) a small-scale Interdigitated Electrode (IDE) microchip system. Surface areas and gap sizes of the various probes were also evaluated to determine their effect on measuring sensitivities. In both series of tests, *Pseudomonas.putida* was used as the model bacteria due to its ability to grow rapidly as a biofilm former, and is commonly found in MIC related environments.

Upon the introduction of the microorganism to the system, EIS patterns collected were correlated to the observed bacterial concentration over time. A model circuit was also developed to determine the effective capacitance and resistances at various bacteria concentrations. Both the parallel plate and IDE systems were able to detect changes in total bacteria concentration (planktonic and sessile) when a threshold value of 10^8 CFU/ml and 10^4 CFU/ml was reached, respectively. The effect of the surface area and gap size was seen to play a role in the effective capacitance value obtained during the test. For the parallel plate probe, the 0.5 mm gap size and 2

cm^2 surface area had a slightly better response. IDEs made with gold conductors and a gap size of 5μm also had a better response compared to IDE configurations. This "proof of concept" study has demonstrated the potential for a viable, real-time detection method for systems susceptible to bio-fouling and/or MIC.

PREFACE

This thesis is an original work by Yongxu Chen. Portions of this thesis have been published in the following refereed conference proceedings (Y. Chen was lead author of this work):

Chen, Y., Derik Vand, P., Haile, T., Wolodko, J. (2020). Detection of biofilm forming microbes using electrochemical methods. *CORROSION 2020 Conference Proceedings, Paper C2020-15087*, NACE International, Houston, TX. 14 pages.

ACKNOWLEDGEMENTS

TABLE OF CONTENTS

LIST OF FIGURES

LIST OF TABLES

1. INTRODUCTION

1.1 Microbial Induced corrosion in pipelines

The global demand for oil and gas has grown doubled since 1965, with a 20% increase in the last two decades to the current level of around 82 million barrels per day [1]. Currently, oil and gas makes up approximately 53% of the world's primary energy supply; within that, Canada has 179 billion barrels of useful bitumen making it 3rd in proven oil reserves amongst other nations [2,3]. To distribute these reserves, over 840,000 km of pipelines are operating in Canada to transport oil and gas to both international and domestic markets [4]. The safety of this vast transportation system is considered very important to the well-being of the Canadian public and the environment. However, with that importance in mind, major oil spills still occur, resulting in potential environmental damage and significant economic loss [5]. From a 2016 study [6], corrosion was found to be a major cost to the oil and gas sector accounting for a significant $2.5 trillion US globally which does not even include indirect costs such as personnel safety and environmental consequences.

Microbiologically Influenced Corrosion (MIC) is a major cause of corrosion failure creating concerns for fluid systems in various industrial sectors (e.g. oil & gas, utilities, mining, etc.). MIC usually occurs as the result of the formation and accumulation of the biofilms/ microbial cells on the surface of the piping systems, tanks, and vessels. These biofilms often include both biotic components (e.g. microorganisms such as bacteria, archaea and fungi) and abiotic materials (e.g. inorganic solids) [7]. These biofilms adhere to the inner wall or surfaces of fluid systems, and develop over time depending on surrounding conditions (i.e. availability of nutrient sources, flow conditions, chemical composition). The formation of biofilms and deposition of solid with their

metabolism (H_2S, extracellular EPS) in systems can eventually lead to the degradation of assets due to MIC, as well as possible reductions in process efficiencies due to the accumulation of biomass (i.e. biofouling). These issues are often detected during routine inspection procedures, or eventually lead to operational upsets such as an unexpected system closure due to a corrosion failure or flow blockage.

1.2 Detection of the MIC

As biofouling and MIC are a persistent issue, the cost to mitigate is high due to regular sampling, inspection, and maintenance. The current MIC detection method relies on sampling and analyzing fluids, solids, or mixture collected in pipelines using lab-based culturing or analytical techniques such as Biological Activity Reaction Tests (BARTs) and Most Probable Number (MPN) bottles. These tests are labor-intensive and time-consuming (up to 30 days for analysis) which can delay mitigation responses. More advanced techniques such as Molecular Microbiological Methods (MMM) can also provide more detailed information about microorganisms present in the system (such as community analysis) but are not as widely used due to lack of training and increased cost [8].

On-line (in-situ) measurement systems have been suggested as an alternative to conventional lab testing by providing real-time results which would significantly improve mitigation response times. Online probes are commonly used by industry for the detection of other (non-MIC) corrosion threats, but there are very few commercial technologies available to detect biofilm formation and/or MIC in a fluidic environment. Several techniques, however, have been

proposed in the academic literature based on a variety of measurement principles (a comprehensive review of these techniques is provided in Chpater 2):

- The intensity of light (Differential Turbidity) [9]

- The intensity of sound (Ultrasonic Frequency Domain Reflectometry or Ultrasonic Time-Frequency Domain) [10]

- Color/wavelengths (Bioluminescence, Fluorometry, Spectroscopy) [11]

- Mechanical resonance frequencies (Quartz Crystal Microbalance) [12]

- Light refraction indices (Attenuated Total Reflection Infrared, ATR-IR spectroscopy) [13]

- Nuclear Magnetic Resonance (NMR) [14]

- Electrical conductivity (Electrochemical Electrodes) [15]

- Electrical capacitance (Dielectric Sensor) [16]

Most of these techniques are either too expensive to practically implement or have not been commercialized due to technical issues [17]. However, electrochemical based probes used in corrosion monitoring have existed for years and are widely available. Furthermore, when these probes are coupled with techniques such as Electrochemical Impedance Spectroscopy (EIS), they provide accurate and detailed information about potential corrosion mechanisms and have been widely used in studies such as the evaluation of corrosion inhibitors [18].

1.3 Objectives of this Thesis

This thesis aims to assess a novel electrochemical-based method to detect and continually monitor bacteria concentrations in a liquid environment based on the EIS technique. Since bacteria cells can exist in either planktonic or sessile forms, this thesis examined two probe types: 1) custom-built parallel plate system to measure total bacteria concentration (planktonic and sessile), and 2) a small-scale Interdigitated Electrode (IDE) system to measure the bacteria concentration under planktonic and sessile conditions. EIS patterns and derived calculated parameters were correlated to the observed bacterial concentration (planktonic or sessile), which was determined using plating methods to quantify microbial counts over time. Surface areas and gap sizes of the various probes were also evaluated to determine their effect on measured sensitivities.

1.4 Thesis Content

This thesis consists of 6 chapters: Chapter 1 is the introduction; Chapter 2 is a review of pertinent literature with respect to MIC mechanisms, detection, and mitigation; Chapter 3 discusses the methodologies used in the three experimental designs used in this study; Chapter 4 presents and discusses the results obtained from the three test setups; and Chapters 5 and 6 present the overall conclusions and future work, respectively.

2. LITERATURE REVIEW

2.1 Microbial Influenced Corrosion

2.1.1 MIC Mechanisms

Microbiologically Influenced Corrosion (MIC) is a complex form of localized corrosion caused by microorganisms' activity on a metallic substrate. Although the mechanisms of the MIC are still not fully understood [19], there are three common mechanisms that have been proposed: 1) the creation of electrochemical cells due to formation of biofilms, 2) the development of corrosive substances produced by the metabolites of microorganisms in a biofilm, and 3) accelerated corrosion due to synergistic effects of various microorganisms in a biofilm.

For the first case, biofilms are created as a result of the attachment of free-floating microorganisms in a fluid (referred to as "planktonic" cells) onto a surface to produce a biofilm or an agglomeration of microorganisms (referred to as "sessile" cells). These attached microorganisms will reproduce and grow under favorable environmental conditions. Over time, the growing biofilm prevents the diffusion of oxygen resulting in anaerobic conditions at the metal surface. As a result, a differential electrochemical cell is set up between the metallic area under the biofilm (which becomes anodic) versus the aerobic surface outside the biofilm (which becomes cathodic) [20]. The anodic site will produce metal ions to form hydroxides which can alter the pH at the interface. This will eventually form a galvanic cell in some cases and will initiate localized corrosion in the form of pits [21].

The second case involves the metabolic substances produced in the biofilms via microbiological activity that leads to corrosion at the metal surface. For example, Sulfate Reducing Bacteria (SRB) are common MIC related microorganisms which obtain energy from organic matter and produce H_2S through the reduction of sulphate ions [22]. The produced H_2S will react with iron on the metallic surface to form Fe_xS_y (black corrosion product). If oxygen is present, the Fe_xS_y will oxidize to generate Sulphur (S), which in turn reacts with iron to form more FeS (further accelerating the corrosion effect). This process is called "Chemical Microbially Influenced Corrosion" (or CMIC) and is the predominant mechanism for SRB induced corrosion [23].

The third case involves the synergistic effect of the diverse microbiology communities within a biofilm which can contribute to and accelerated corrosion effects. Methanogenic archaea (MA) are an example of a microorganism that is often found in conjunction with SRB in offshore systems, and will accelerate MIC through the process of methane formation. Methane is initially formed by MA through the oxidation of iron (iron sulphate) from carbon dioxide. This process accelerates corrosion by releasing the electrons from iron through dissolution during the above reaction. As a result, MA and SRB work together to accelerate corrosion using their respective reactions [24]. Other synergistic mechanisms, however, are complex and have not been fully characterized for MIC related microorganisms (area of active research).

2.1.2 Biofilm Development

A biofilm is a group of microorganisms where microbial cells adhere to one another and to substrates (such as metals, plastics, concrete, etc) to form a complex mass and community of cells. These cells are encapsulated and bound within a slimy matrix composed of extracellular polymeric substances (EPS). The EPS is produced by the cells within the biofilm, and are a polymeric conglomeration of extracellular proteins and polysaccharides [25].

Before a mature biofilm is formed on a surface, microbial cells pass through several steps. The initial seed of cells within a biofilm are from planktonic communities which are cells found floating in suspension in a fluid. These cells eventually attach themselves onto a solid surface, and forms a sessile microbial community. When the nutrients in the sessile microbial community becomes exhausted, the microbial cells on the top layers will begin to peel off and migrate to new landing sites.
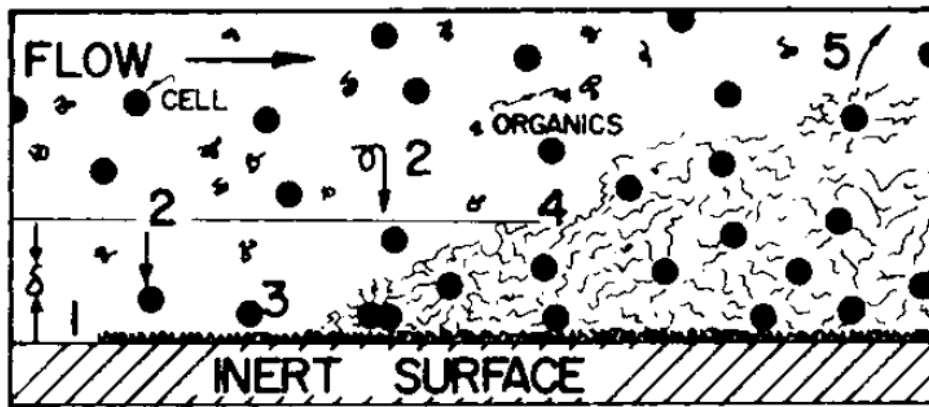
Figure 1. The different stages of biofilm formation [26][1]

Referring to the notations in Figure 1, the main stages of biofilm formation are as follows [24]:

---

[1] Figure reproduced with permission.

1) Transport Stage - Transport of organic and inorganic materials from the bulk fluid to the pipeline surface.

2) Adsorption Stage - Adsorption of the materials to the wetted surface resulting in a conditioned surface. The site of cell attachment is based on the local flow conditions (i.e. laminar flow) and the effect of gravity (stagnant or low flow conditions are preferable for biofilm formation). There are some studies that have shown that anodic points on the metal surface will attract cells as a result of micro-flaws during the manufacturing of the material.

3) Reversible Adhesion Stage - The adhesion of microorganisms within the biofilm and on surface is weak, and can be removed by fluid flow. The weak adhesive forces are usually a result of electrostatic forces, Van der Waals forces, interfacial tension, and/or covalent bonding.

4) Irreversible Adhesion and Growth Stage - Microbial cells are equipped with a molecular signaling system that allows the organisms to sense their environment and regulate their reproduction rate (quorum sensing). This signal also triggers the reorganization of cellular machinery in the bacterium. Microbial cells produce thin fibres (called "pili") which extend from the cell to assist with adhesion to the substrate. This can be observed when multiple cells are in contact with one another [27]. Once the bacteria positions themselves, they secrete EPS which enhances bonding of the cells together and to the substrate, and provides a barrier to external conditions (e.g. shear forces, biocides, and others). The biofilm matures when the cells are fully embedded in the EPS matrix [28]. At maturity, the biofilm is a complex structure of colonies, pores and polymers.

5) Decay and Detachment Stage - As oxygen and nutrients are depleted in the mature biofilm, it may start to decay. Cells in the upper layer, which can still access nutrients, may detach

from the biofilm to form free-floating cells. These planktonic cells seek new sites for biofilm initiation and growth, restarting the five growth stages described above [26].

2.1.3 Mitigation of MIC Threats

There are various approaches to mitigate MIC threats in practice. The main objectives of these mitigation strategies are to either eliminate or disrupt microbiological activity, or reduce the corrosion effect on the metallic surface. In general, there are several methods used to mitigate MIC in oil and gas systems including mechanical cleaning (pigging), biocides, corrosion inhibitors, use of non-metallic piping, and cathodic protection. Details of these five strategies are outlined in the following sections.

2.1.3.1 Mechanical Cleaning (Pigging)

Mechanical cleaning (also known as "pigging") is one of the most common corrosion mitigation methods currently used to prevent MIC in the pipeline industry [29]. The etymology of "Pigging" has different origins, and one of them stands for "Pipeline Inspection Gauge (pig)". A cleaning pig is usually a cylindrically shaped device with a rounded end that is placed inside the pipeline to clean the pipe inner surface. The pig's outside diameter is a close fit with the pipe inner diameter which allows it to be propelled down the pipeline by fluid flow (applied differential pressure). The outer surface of the pig often contains ridges or bushes which can remove solid deposits, wax buildup and/or biofilms on the inside surface of the pipe as the pig moves through the system. Pigs are usually inserted and retrieved from pipelines using a pig "launcher" and pig "catcher" which are specialized fittings (laterals) that are built-in to a pipeline system at specific locations to facilitate regular maintenance runs. Cleaning pigs can be typically used on pipelines

with a nominal diameter of 50 mm (2 in.) or greater. It is a very effective method to remove biofilms/deposits in a system at regular intervals, thus mitigating MIC threats.

2.1.3.2 Biocides

Biocides are a type of corrosion control chemical specifically used to mitigate MIC related threats. Biocides act to reduce or eliminate microorganisms in oil and gas systems by affecting the general functionality of living cells, ultimately resulting in their death. A number of biocide chemistries have been developed over the years to target specific microorganisms and environments (there is no single biocide chemistry for all conditions). Biocides can be injected as liquids into a variety of petroleum production systems using one of two methods: 1) batch treatment or 2) continuous injection. For the "batch treatment" method, a large single dose of biocides is injected into either a dynamic (e.g. pipeline) or stagnant (e.g. storage tank) system to reduce or eliminate MIC related microbial populations. These batch processes are often repeated at regular intervals (e.g. weekly or monthly) in order to mitigate MIC threats. For the "continuous" treatment method, the biocide is continuously injected (gradually) into a system at much lower concentrations relative to the batch method, and is common in flowing pipeline systems to maintain low microorganism counts. One challenge with biocide use is potential environmental toxicity and disposal. In addition, biocidal effectiveness and persistency should be considered when choosing a biocide in order to prevent biocide resistance over time.

2.1.3.3 Corrosion Inhibitors

Corrosion inhibitors are another form of corrosion control chemicals which act as a temporary chemical film on the pipe interior which reduces the potential for corrosion by isolating any water in the system from the metal surface. It is most commonly used to mitigate abiotic corrosion threats, but has also been used for cases where MIC can be present. Corrosion inhibitors are designed to adhere to metal surfaces, and can be based on organic or inorganic chemistries. Corrosion inhibitor molecules typically consist of two parts: 1) a ring-based head group that bonds (via adsorption) on to the metal surface, and 2) a hydrophobic chain (water repelling) facing away from the metal surface. The hydrophobic chains will attract other hydrophobic molecules in proximity and form a film making the metal surface inaccessible to water, thus preventing conditions for corrosion to occur. The ring-base head group will also form a film on the metal surface to provide extra isolation [24]. Corrosion inhibitors are typically applied by direct injection into the pipeline fluid, or by using a pipeline "filming pig" to apply an even coat to the inside surface of the pipe. The selection of corrosion inhibitors is based on specific the corrosion mechanism diagnosed and the environmental/operating conditions of the system (e.g. fluid type, temperature, pH).

2.1.3.4 Use of Non-metallic Piping and Coatings

Non-metallic piping (e.g. polymer or composite materials) and internally coated steel pipe are often used in oil and gas systems which experience regular or severe corrosion problems from either abiotic or biotic (MIC related) threats. It is becoming a popular alternative to small diameter steel flowlines which are typically too small to clean using pigging methods (e.g. pipes less than 50 mm nominal diameter). Non-metallic alternatives typically have higher capital costs compared

to steel piping, but may have a lower overall life-cycle costs due to the elimination of corrosion control chemicals (biocides or corrosion inhibitors). Common non-metallic materials include polyethylene (PE) liners, fusion bonded epoxy (FBE) coatings, polyurethane (PU) coatings, and glass-fiber reinforced polymer (FRP) composites.

2.1.3.5 Cathodic Protection

Cathodic protection (CP) is another mitigation method commonly used in buried oil and gas infrastructure to reduce or prevent corrosion by disrupting/changing the electrochemical potential of the metal surface. This is accomplished by loading the metal surface with electrons to favor metallic iron when sufficiently negative potential can be reached. For buried structures (such as pipelines), cathodic protection systems essentially create an electrochemical cell by burying a metal with a higher electric potential (anode) near the structure (cathode), and attaching an insulated conducting wire between them. The soil acts as the electrolyte to transfer ions between the structure and the anode metal, thus closing the circuit. The anode is designed to have a higher electrical potential relative to the metallic structure (e.g. steel), thus preventing corrosion or electrochemical degradation to the structure surface. In practice, there are two main types of cathodic protection: 1) galvanic, and 2) impressed current. For galvanic cathodic protection, the anode consists of a sacrificial metal such as zinc, aluminum or magnesium. These anodes physically degrade over time and need to be replaced at regular intervals (e.g. months or years) to maintain protection to the structure. For the impressed current method, an external source of electrical power is used with a permanent (inert) anode to alter the electrochemical potential in the system. Impressed current systems offer higher voltages and lower maintenance relative to galvanic systems but require access to a reliable source of electricity. Cathodic Protection is a commonly used method on large diameter pipelines, and is effective at reducing external corrosion

especially when used in conjunction with external coatings. It is reported that in a system with electron-accepting microorganisms present, the protective potential will be lower compared to the system without those microorganisms to accommodate the extra electron accepting capacity.

2.2 Offline Biofilm Detection

There are two general approaches for detecting and quantifying microorganisms in oil & gas systems: a) the sampling and testing of pipeline fluids or solids (sludges), and b) the use of retractable test coupons/probes in a pipeline. For the first approach, fluid samples can be collected during pipeline operations (drain ports) while solids are collected during mechanical cleaning operations (i.e. pigging). The samples are then analyzed in a lab using culture base methods such as serial dilution bottles or Biologically Active Reaction Testing (BART). Both employ color changes as a means to confirm and quantify the presence of specific microorganisms in the sample. Various MIC related microbial functional groups can be detected using these methods including Sulfate Reducing Bacteria (SRB), Acid Producing Bacteria (APB) and Iron Reducing Bacteria (IRB). These tests can be performed under aerobic or anaerobic conditions. The main challenge with this approach is that the samples collected (fluid or solids) are conglomerations and mixtures of fluids or solids taken along some length of the pipeline, rather than at a discrete location. As a result, specific microbiological characteristics may not be fully representative of sites where MIC occur.

For the second approach, retractable coupons/probes can be inserted at specific locations in pipeline systems which provides a substrate or surface for biofilms to form. These probes can be placed directly in the fluid flow, or flush with the pipe inside surface. The advantage of this method is that these probes can be removed at regular intervals in order to sample biofilm residue

at the surface of the associated coupons (i.e. using swabs). Various techniques can be performed on these samples including the aforementioned culture-based methods, in addition to more advanced techniques such as microscopic imaging. The main advantage of this approach versus sampling fluid/solids from maintenance runs is that the biofilm on probes represent localized bacteria communities (versus an agglomeration along the pipe length).

These approaches are both considered "offline" monitoring techniques since the detection of microorganisms occur by post-processing the acquired samples. The final characterization is often performed at an offsite laboratory, and can often take several days/weeks to obtain results. A summary of currently available commercial offline monitoring methods is provided in Table 1.

Table 1. Current offline monitoring tools.

Method	Approach
Serial Dilution Bottles	Sampling
Biologically Active Reaction Testing (BART)	Sampling
Bio-Probe HCA200	Coupon
ROHRABACK COSASCO Bioprobe	Coupon
CAPROCO BIOFILM SPOOL	Coupon
CorrOcean Biofilm probe	Coupon

2.3 Online Biofilm detection

Numerous approaches for detecting the presence of microorganisms or biofilms directly in fluid systems in real time have been proposed over the past few decades. The advantage of these online approaches is their ability to detect microorganisms in-situ (in the fluid system being considered) and in real-time without the need for post-processing samples (i.e. lab tests). These systems allow operators of pipelines to respond more rapidly to changes in microorganism count which may reflect possible threats due to MIC or biofouling.

Most online biofilm monitoring methods/tools measure presence of microorganisms or biofilms based on changes to various types of applied or passive signals. These are affected by the presence of microorganisms themselves or based on components within biofilms (e.g. EPS, proteins, cells, genetic materials, etc). The output signals constitute energy transfer, such as radiation (including light), acoustic waves, electrical fields, electric current, or heat transfer. Only very few of these signals are directly emitted by the biofilm (e.g. bioluminescence); most of the signals are a passive response to input signals generated by the monitoring equipment. In the latter case, input signals are transmitted to the surface of a biofilm and are modified in response to the presence of biological components (EPS, protein, bacterial cells, etc.). The output signal (response) is compared with a base signal from a surface without biofilms. Various signal sources and detection principles have been studied including the intensity of light (Differential Turbidity), the intensity of sound (Ultrasonic Frequency Domain Reflectometry or Ultrasonic Time-Frequency Domain), color/wavelengths (Bioluminescence, Fluorometry, Spectroscopy), mechanical resonance frequencies (Quartz Crystal Microbalance), electrical capacitance (Dielectric Sensor), electrical conductivity (Electrochemical Electrodes), light refraction indices (Attenuated Total

Reflection Infrared, ATR-IR spectroscopy), and Nuclear Magnetic Resonance (NMR). Each of these approaches are described in the following sections.

2.3.1 Fluorescence spectroscopy

Fluorescence spectroscopy is an analysis of the fluorescence emitted from a sample (i.e. biofilm) after excitation provided by a shorter wavelength light source, usually ultraviolet. It is primarily associated with electronic and vibrational states of the electrons from the molecules in the cells embedded in the biofilm, also referred to as the electron energy levels (within each of these electronic states, there are a number of vibrational states). Prior to excitation, the biofilm molecules have electrons that are in a ground electronic state (low energy level). Upon application of an ultraviolet light source, the molecules are excited by photon absorption and the electrons move from the ground state to one of the various vibrational states (higher energy level). Collisions of these excited molecules cause them to lose vibrational energy, and eventually drop down to lower energy levels until again reaching the ground electronic state. In the process of losing this energy, a photon is emitted, with a wavelength proportional to the respective energy gap in the return to the ground state.

An analysis of the different frequencies of light emitted in fluorescent spectroscopy, along with their relative intensities, can be used to infer the structure of the vibrational levels in the biofilm. Each fluorescent molecule has its own characteristic excitation and emission frequency, usually within the fluorophores ultraviolet light excitation wavelength range. Fluorophores absorb the energy from the UV light, resulting in the transition from the ground state to a higher excited electronic state. When the UV irradiating source ceases, the electrons in the fluorophores will return to the ground state while emitting photon energy in the form of light [11].

Each fluorophore type has a unique fluorescence spectrum, and by monitoring the intensity and the wavelength of the fluoresce spectrum, types of fluorophores in the sample and their change in concentration can be monitored [30] The spectrum could be collected in either 2-D (i.e. excitation spectrum) or 3-D with a range of excitation wavelength and emission wavelength along with intensity value shown as Figure 2 below. With a 3-D spectrum, some more qualitative information would be monitored as sometimes more than one fluorophore is involved.
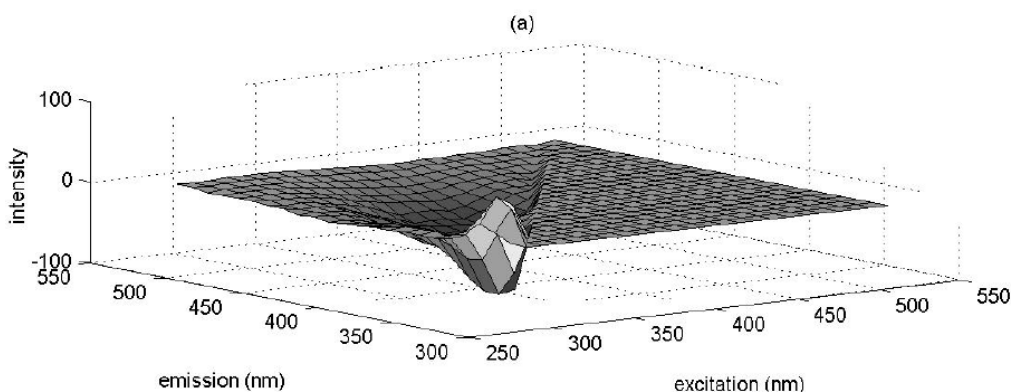
Figure 2. 3-D fluorescence map of a mixed species DCE degrading biofilm using tryptophan as a fluorophore [31][2].

Common biomolecules fluorophores include the aromatic amino-acid Tryptophan and nicotinamide adenine dinucleotide phosphate [NAD(P)H]. Tryptophan absorbs ultraviolet around 280 nm, and a photon of light is emitted with a wavelength around 350 nm. [NAD(P)H] absorbs UV light around 366nm and then emit fluoresce around 450nm [32]. Both these molecules exist in most cell mitochondrion, so it is very helpful to use them as a built-in fluorophore to conduct the analysis.

---

[2] Figure reproduced with permission.

Quantifying the relationship of the fluorescence and the concentration of specific species can be described using the Beer-Lambert Law, as shown in Equation 1 [11]:

$$f = I_0(1 - e^{-kCL})\varphi_f \qquad (1)$$

where f is the total fluorescence, I_0 is the irradiating UV light intensity, k is the molar extinction coefficient, C is the concentration of the absorbing species, L is the light path of the absorption, and φ_f is the fluorescent efficiency of the fluorophore. The fluorometric emission of light at a specific wavelength following excitation is usually measured by a sensitive photo-multiplier tube (PMT) with a narrow pass band filter mounted in front. With the constant UV light input, the change of f can be correlated with C. The cells can also be stained by using commercially available kits and then observed under a fluorescence optical microscope to give a more direct measure of the cell concentration in the biofilm [33].

2.3.2 Photoacoustic spectroscopy

The generation of sound when a material is illuminated with non-stationary light is called the photoacoustic (PA) effect. It was first discovered by Alexander Graham Bell in 1880 [34]. Photoacoustic Spectroscopy (PAS) is the application of the PA effect for spectroscopic purposes [35]. PAS can be used to monitor biofilm growth where electromagnetic radiation is absorbed by the biological sample, and a non-radiative relaxation process within the samples converts the absorbed energy into heat. The thermal expansion and contraction of the biological medium generate a pressure wave detected by microphones or piezoelectric transducers [36]. When using lasers as the light source, this is referred to as Laser Photoacoustic Spectroscopy (LPAS). The interaction of the photons within the material subject to electromagnetic radiation may produce a series of effects.

When the incident photons are absorbed by the biofilm, internal energy levels within the biofilm are excited. The excited state may lose its energy by radiation (spontaneous or stimulated emission); and/or by non-radiative deactivation, which channels part of the absorbed energy into heat and generating a pressure wave. In solid samples (e.g. biomaterials, biofilms), the heat is stored as vibrational energy in the ions or atoms.

The distance between an absorbing object inside the sample and the sample surface can be calculated as the product of the speed of sound and time travelled. Thus, changes in the optical absorption properties of a sample can be investigated depth-resolved, if the sound velocity inside the sample is known. The amplitude p of a photoacoustic signal generated by a laser pulse inside the samples can be generally described as shown in Equation 2:

$$p \propto \frac{\beta c^2}{c_p} E_0 \mu_a \qquad (2)$$

Where C_p is the heat capacity, β is the thermal expansion coefficient, c is the speed of sound in the biofilm understudy, E_0 is the laser pulse energy, and μ_a is the absorption coefficient of the sample [37]. If a short laser pulse is used for excitation, a time-resolved recording of the photoacoustic signal allows a depth-resolved investigation of the light absorption inside the irradiated part of the sample [38]. The absorption coefficient can be determined by UV-Visible Spectrometry.

PAS allows the non-destruction monitoring of biofilms by measuring the photoacoustic absorption in the visible spectra range (λ =400nm~700nm) to monitor the growth, detachment and thickness of biofilm [39].

2.3.3 Magnetoelastic effect (Inverse magnetostrictive effect)

The characteristic resonance frequency of certain metal material will vary when stress/strain was applied to it due to the magnetic field change. This idea may be adopted to place ribbon-like magnetostrictive material inside the reactor as a sensor. The resonance frequency will be different as biomass begins to attach on the surface. This can be detected using a time-varying externally applied magnetic field [40].

In operation, excitation magnetic field frequency is swept over a range of frequencies, inducing a mechanical vibration in the ribbon-like sensor. This, in turn, gives rise to a time-varying magnetic flux that reaches a maximum when the frequency of the excitation magnetic field reaches the fundamental resonance frequency of the sensor. This magnetic flux can be detected and converted into an electrical signal by the use of a pick-up coil. No physical connections between the sensor and the monitoring system are required for signal detection, nor does the sensor require an internal power source. This ability to monitor vibration remotely without a direct physical connection makes it attractive for in-situ and online in vivo monitoring applications. Magnetoelastic sensors are always made of amorphous ferromagnetic ribbon (eg. Metglas® alloys 2826MB and 2605SC) [41].

The sensor placed in the flow cell has a unique resonance frequency as shown in Equation 3:

$$f_r = \sqrt{\frac{E}{\rho}} \frac{1}{2L} \tag{3}$$

Where f_r is the resonance frequency, E is Young's modulus and ρ, L are the solution density and sensor's length, respectively. When biomass is deposited on the sensor, the resonant frequency will shift depending on the mass deposited as shown in Equation 4 [42].

$$\Delta f = \frac{-f_r \Delta m}{2m_0} \tag{4}$$

Which m_0 is the initial mass and Δm is the mass change during the process. In addition to the frequency shift, the change in amplitude is also an indication of biomass activities. Lakshmanan et al showed the frequency change could be correlated with *salmonella typhimurium* using a sensor length of length 2mm in Figure 3. Although no quantitative relation has yet been published, Pang et al found the amplitude shift is almost related to biomass mass thickness change while frequency change is depending on viscosity and biomass in *P. aeruginosa* [40].

The relation between viscosity and mass attached with resonance frequency was shown in Equation 5:

$$\Delta f = -\frac{\sqrt{\pi f_0}}{2\pi \rho_s d}(-\eta \rho_1)^{\frac{1}{2}} \tag{5}$$

Where f_0 is the resonant frequency of the sensor in air; ρ_s and d the density and thickness of the sensor; ρ_1 and η are the density and viscosity of the liquid [41].
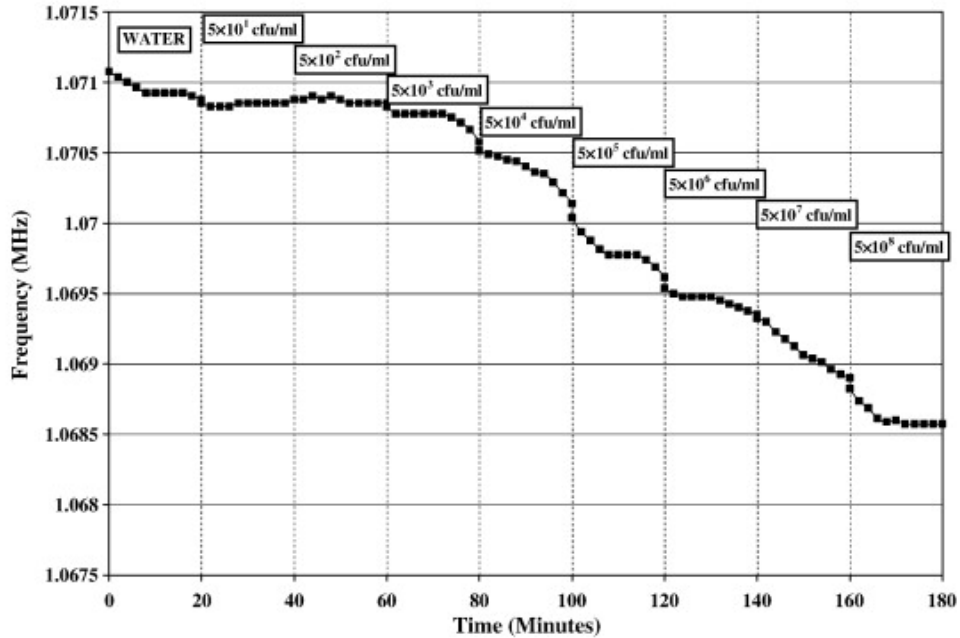
Figure 3. Dynamic response curve for a magnetoelastic strip with 2*0.4*0.015mm with salmonella [43][3].

This method has a simple setup and has the potential to have a quantitative measurement of the biomass attachment. The change of the frequency and amplitude and its relation make it possible to monitor both planktonic cells and sessile biomass. However, the distribution of viscosity changes and biomass attached needs further study as there might be some synergy between these effects. Ong et al have also reported the magnetoelastic effect can also be used to measure several bioagent concentrations quantitatively with the help of antibodies [44].

2.3.4 Ultrasonic Methods

When a longitudinal sound wave travels through a medium and reaches an interface with a second medium, the sound wave can be partially reflected or transmitted. The reflected portion

---

[3] Figure reproduced with permission.

of the incident wave produces an echo. The reflecting interface can result from two distinct layers of media, flaws in the material and porous in the medium [45]. Distribution of the transmitted and reflected wave is determined by the acoustic impedance mismatch (incident beam perpendicular to the interface) as shown in Equation 6:

$$R = \frac{z_2 - z_1}{z_2 + z_1}; T = \frac{2z_2}{z_2 + z_1}; R + T = 1. \tag{6}$$

Where z_1 and z_2 are the respective acoustic impedances of the two media, R is the reflection ratio, and T is the transmission ratio of the wave. This is the simplest form of the relation for the case of the wave at normal incidence. Acoustic impedance (Z) is typically measured in units of rayls (Pa* s/m) and physically represents the ratio of sound pressure to particle velocity at a point in a given material. Z is defined as the product of density and acoustic velocity in the medium as shown in Equation 7 [46]:

$$Z = \rho c \tag{7}$$

Typical value for acoustic impedance in dry air (0^oC): 0.4286 Krayl; liquid water at $20C^o$: 1.494 Mrayl; Aluminum 17.33 MRayl; Tungsten 101 Mrayl. Knowledge of velocity of sound in different media allows for the calculation of the distance between the interface(s) and the transducer. In practice, there are two methods for monitoring biofouling by the ultrasonic principle: Ultrasonic time-domain reflectometry (UTDR) and ultrasonic frequency-domain reflectometry (UFDR).

2.3.4.1 Ultrasonic time-domain reflectometry (UTDR)

Ultrasonic time-domain reflectometry (UTDR) is a reflectometry that instantaneous amplitude of reflected wave excited from ultrasonic-wave is recorded as a function of time [47].

For a typical ultrasonic setup of biomass thickness detection, a biofilm is first formed on a substrate in a closed chamber filled with liquid. The transducer is then placed on the bottom of a substrate, and the sound wave excited by the transducer will first encounter the top of the substrate resulting in the first echo. If no biofouling has occurred, the sound wave will reach the top of the container result in a second echo. With bio-fouling present in the system, there will be another interface between biofilm and the solution (the third echo will appear as the addition of the interface). If the thickness of the biofilm changes, there will be a shift of the third echo wave (the shift in time is dt). The thickness of biofouling ds can be determined by equation 8:

$$dt= 2ds/v \qquad\qquad (8)$$

Where v is the velocity of sound in the fluid medium [48]. Besides the shift of the arrival time, the amplitude of the echo wave is also observed, Hou et al [49] tested the amplitude increased as of $CaSO_4$ deposit on biofilm fouling at different times.

2.3.4.1 Ultrasonic frequency-domain reflectometry (UFDR)

Ultrasonic frequency-domain reflectometry (UFDR) is a reflectometry method that measures the amplitude of the reflected wave as a function of frequency. When there are multiple reflections in the setup, many overlaps or noise is present such as irregular shape of the container or multiple interfaces in the biofilm. When the clear reflected wave is difficult to distinguish, the characteristic of the fouling or defects of the material can be identified using frequency-domain reflectometry. Compared to UTDR, UFDR is capable of characterizing the size and shape of the pores. By applying the UFDR, these characteristics are revealed by ultrasonic response at different frequencies [46].

To quantify the characteristic signal for UFDR, the total reflected power (TRP) method can be used. The TRP from each acoustic observation is found by integrating the amplitude over a frequency range (e.g. 0~10 MHz) as proposed by Kujundzic et al [45]. The amplitude of the signal A, of the reflected wave relative to the incident wave is given by Equation 9:

$$A = \frac{Z_2 - Z_1}{Z_2 + Z_1} \qquad (9)$$

Where Z_1 and Z_2 are the impedance between different mediums as discussed above. Significant variability in the TRP values may be attributed to the fact that biofilms are dynamic in nature with their properties and morphologies constantly changing. Figure 4 from Kujundzic et al shows a distribution of TRP power of extracellular polysaccharides deposited on Polyvinylidene Fluoride (PVDF) microfiltration membrane coupons. TRP values with a unit of (V*MHz) for a number of observations from different biomass levels was listed. As the extracellular polysaccharides (EPS) concentration increased, the peak of the TRP value shifts to the left as the TRP value decrease as the amplitude was hindered by the biomass.
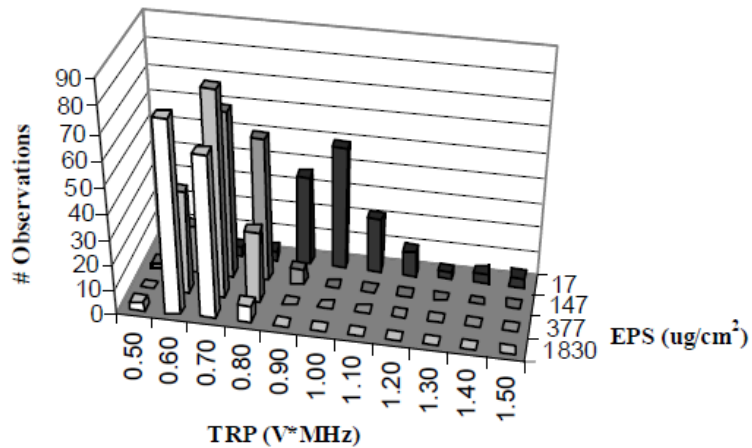
Figure 4. Distribution of the total reflected power from polyvinylidene fluoride microfiltration membrane coupons [10][4].

---

[4] Figure reproduced with permission.

2.3.5 Quartz Crystal Microbalance (QCM)

Quartz crystals are piezoelectric materials which accumulate electron charges when pressure is applied. Conversely, when an alternating current (AC) is applied, oscillations are induced. By adjustment of the frequency of the AC, the oscillations can be tuned to the crystal's resonant frequency to generate a standing wave. The resonant frequency is dependent on the thickness of the crystal. The addition of mass (i.e. deposition of biofilms) change the crystal's resonant frequency, and these frequency changes can be measured with high precision.

The relationship between frequency change and mass adsorbed is given by Sauerbrey in Equation 10 [50]:

$$\Delta m = \frac{C}{n} \Delta f \tag{10}$$

where n is the harmonic number, (number of the standing wave) and

$$C = \frac{t_q \rho_q}{f_0} \tag{11}$$

where f_0 is the original resonant frequency, t_q, p_q are the thickness and density of the quartz, respectively.

Note, however, that this equation assumes that the mass adsorbed is rigid. For applications of QCM in biofilm monitoring, the biofilm usually consists of an extra polymer layer (macro biomolecules) with viscoelasticity features and a liquid. The non-rigid attached mass also contributes to the frequency change. Hence, an alternative approach for characterizing mass deposits with frictional dissipative losses due to their viscoelastic character was introduced. This method, known as Quartz Crystal Microbalance dissipation (QCM-A), measures the decay of a

quartz oscillation after a rapid excitation close to the resonant frequency is removed. The decay in amplitude decay over time is dependent on the properties of the quartz crystal and the contact medium or adsorbed mass. The amplitude change over time always has a damped sinusoidal pattern. The sinusoidal pattern can be fitted using Equation 12 [12]:

$$A(t) = A_0 e^{t/\tau} \sin(2\pi f t + \alpha) \tag{12}$$

where $f = f_0 - f_r$. f_r is a reference resonant frequency. The dissipation parameter is given by Equation 13:

$$D = \frac{1}{\pi f \tau} = \frac{E_{dissipated}}{2\pi E_{stored}} \tag{13}$$

Where $E_{dissipated}$ is the energy dissipated during one oscillatory cycle and E_{stored} is the energy stored in the oscillating system [51].

If there is only a rigid mass layer attached to the crystal (rigid protein mass), only the frequency will change. However, if a viscoelasticity substance is attached, both QCM and QCM-A will respond to the change. The resolution possible for the measurement of the change in frequency is on the order of ±0.1 Hz, and the dissipation in the liquid is on the order of 1×10^{-7} (dimensionless).

Nivens et al [52] has investigated the change in frequency and established the relation between the frequency change and cell concentration, as shown in Figure 5. This study also compared the frequency shift data for a system with *P.cepacia* bio cells with measurements taken with a sterile control. The sterile control has little shift in frequency while the data taken with bacteria reveals a significant change in frequency over time. The changes in the bacteria curve

begin after 10 hours due to the delay before the attachment of the bacteria to the crystal, as shown in Figure 6.

The combination of QCM and QCM-A provides a non-destructive measurement tool to monitor mass fouling on certain surfaces. The commercial product is already available and on the market.
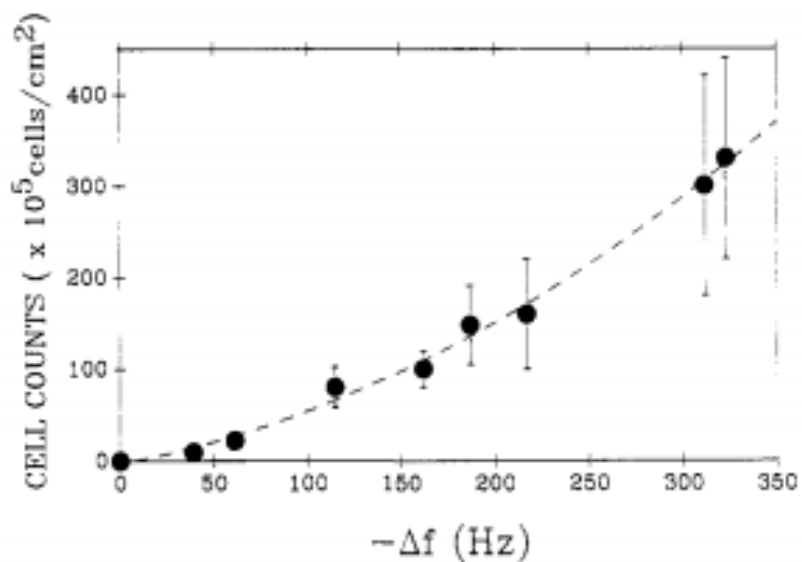
Figure 5. Cells count of attached bacteria within a biofilm versus frequency shift [52][5].
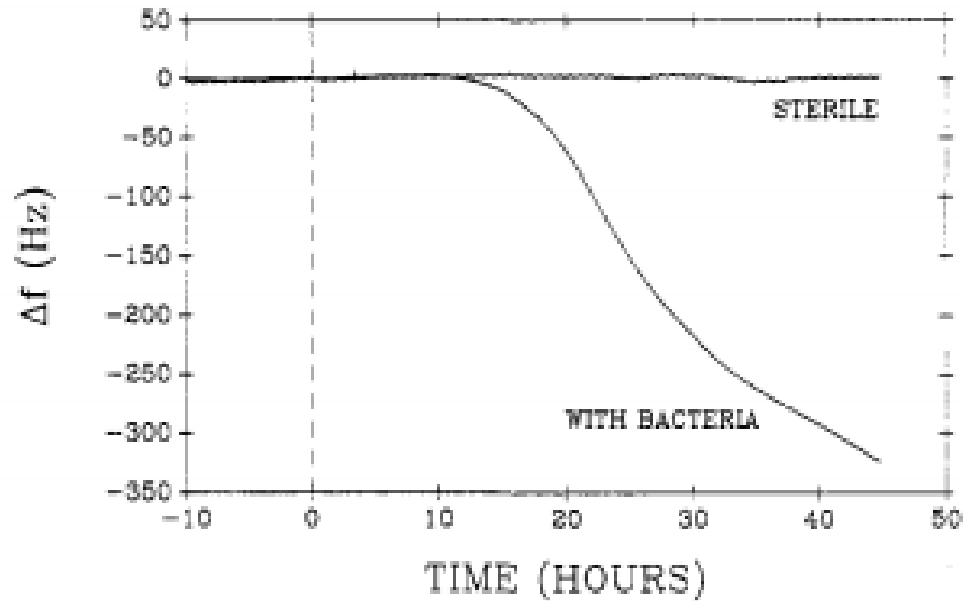
Figure 6. Graph comparing the frequency response of the QCM monitoring a sterile flowing medium versus biofilm reaction [52][6].

2.3.6 Optical Coherence Tomography Method

Optical coherence tomography (OCT) is a technique that can be used to monitor both biofilm thickness and biofilm geometry. OCT is an interferometric technique, typically employing coherent light source, typically in the near infrared. In comparison with optical microscopy in the visible light spectrum, the use of relatively long wavelength light (800~900nm) allows deeper penetration into the biofilm [53].

In operation, a beam of light from a laser diode or other infrared light source split into two beams with a beam splitter, the reference beam and the probe beam. The reference beam is directed to an interferometer while the probe beam is directed to the sample through a scanning mirror.

---

[6] Figure reproduced with permission.

Reflections from the sample interfere with the returning reference beam directed to the photodetector to record an interference pattern. The depth resolution is usually 10μm in commercial systems [54]. Optical coherence tomography can generate images from transparent media with a thickness of several millimetres.

By scanning the sample, a 2D image can be generated over an area from 4 to 100mm^2 depending on the instrumentation available. 3D scans are possible by the assembly of 2D "slices" using commercial 3D software [55].

These systems are capable of scanning the surface of the biofilm quickly, enabling the study of the transient interfacial stages of biofilm growth. The density profile along a dimension can be also displayed which creates a direct view of the distribution of the biofilm.

Since the OCT is performed from the backside of the substrate, it can only measure the sessile cells. If the biofilm thickness is too large, such that the light cannot reflect back to the detector, most of the protons will be scattered. The resolution of OCT is generally 100~400 μm which is inadequate to distinguish single biofilm cells, hence making measurements of the cell concentration difficult.

2.3.7 Attenuated Total Reflection/Fourier Transform Infrared Spectroscopy

Attenuated total reflection/Fourier Transform infrared spectroscopy (ATR/FT-IR) provides a non-destructive method for analysis of biofilms. In solids and liquids, infrared (IR) spectrometry is used to study the interaction between IR radiation and vibrational modes of molecules. IR radiation is absorbed by a molecule when the energy of the radiation is equal to that need to promote the molecule to an excited vibrational state. With this technique, near and mid-

infrared light (wavelength 0.8-25μm) is launched into an internal reflection element (IRE) and is repeatedly reflected as it travels through the IRE to a detector on the opposite end. This is similar in principle to the transmission of light through an optical communications fibre.

At each reflection site along the internal surface of the element, a longitude wave of radiation known as an evanescent wave will penetrate through the IRE into the surrounding flow channel. The evanescent wave is absorbed by the biomass attached to the IRE. The loss of energy at these reflection sites reduces the intensity of the IR radiation arriving at the detector. The typical wavelength range of ATR-IR is within (0.8-25μm). The effect of the energy loss at the reflection sites can depend on the particular molecules/proteins being monitored, thus creates unique "fingerprints" in the collected IR signal at the detector [13]. Background noise is filtered by means of Fourier transformation [56].

The depth of penetration is defined as being the point where the intensity is lowered to 37% (1/e) of its original intensity at the reflection site according to Nivens et al and is defined in Equation 14 [13]:

$$Dp = \lambda / 2\pi n_1 (\sin^2\theta - (n_2/n_1)^2)^{0.5}$$ (14)

Where λ is the wavelength of the radian, n_1 is the refractive index of the IRE; n_2 is the refractive index of the biofilm in contact with the IRE, and the θ is the incident angle as the light beam shoot into the channel similar as an optic fibre. Therefore, once the specific functional group in the biofilm is identified using the IR spectra, the distance of the function group from the IRE surface can be determined. The height of the absorbance peak also reveals thickness information [57]. Based on the equation of the penetration depth, the maximum penetration depth of the IR ray based on its wavelength range (0.8-25μm), should no longer than 1 micron. Nivens et al [13]

have also confirmed that more absorption will be observed as time progresses, as shown in Figure 7. Quiles et al [57] reported that after 30hours, pseudomonas fluoresces biofilm grew to the thickness of 400nm which is still within the detection range of the method.
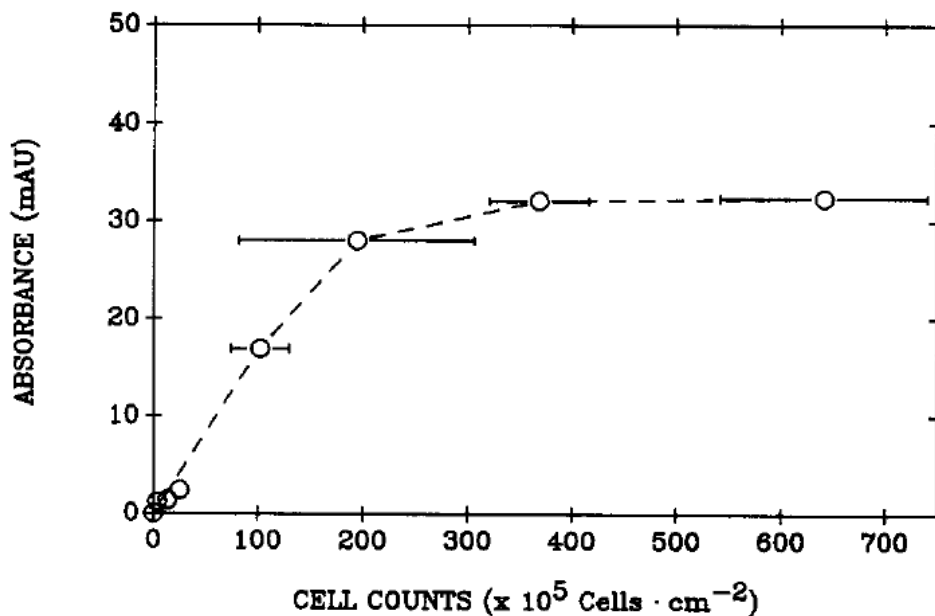
Figure 7. The IR absorbance of amide II band versus the number of cells on the surface of the IRE at different times [13][7].

2.3.8 Visible Light Methods

Visible light (with wavelength 400~700nm) can also be used to monitor biofilms based on the intensity of reflected light scattered due to the uneven surface of the biofilm and turbidity of the solution. This method makes continuous real-time measurements rather than discrete

---

[7] Figure reproduced with permission.

measurements of biofilm. The viability of this method was investigated by Tamachkiarow and Flemming [9].

The optical monitoring system usually consists of 3 parts: a) a transparent medium, b) a visible light source, and c) a receiving detector. The transparent medium can be either beneath the biofilm or in the area around the biofilm. The light source can be either based on fibre optic bundles to source and read the output or based on LED arrays as a source. For the fibre optic bundles, the systems collect light reflected from the biomass while the LED approach is based on light transmitted through the biomass. A photodiode collects the light output for processing [58].

For the system based on biomass reflectance, the growth of biomass will result in more light to be reflected, thereby increasing the output signal. In contrast, for a system based on light transmission through the biomass, the light intensity will be weakened in response to the biofilm growth. The intensity of the light in the transmission method is generally denoted by arbitrary units (AU's) reflecting a relative change in biomass. Meryer et al. [58] used this method and suggested that the Student's t-test be used to distinguish whether changes in intensity were significant or not. Additional data using this method was also collected by adding a biocide to separate the biofilm from the substrate, and measuring the differences in output signal before and after application. The linear correlation between biofilm thickness and light intensity was then established shown in Figure 8.

This method can be easily implemented using inexpensive optical components (ie a light source and a photodetector) with the biofilm growth associated with an increase or decrease in photodetector output.
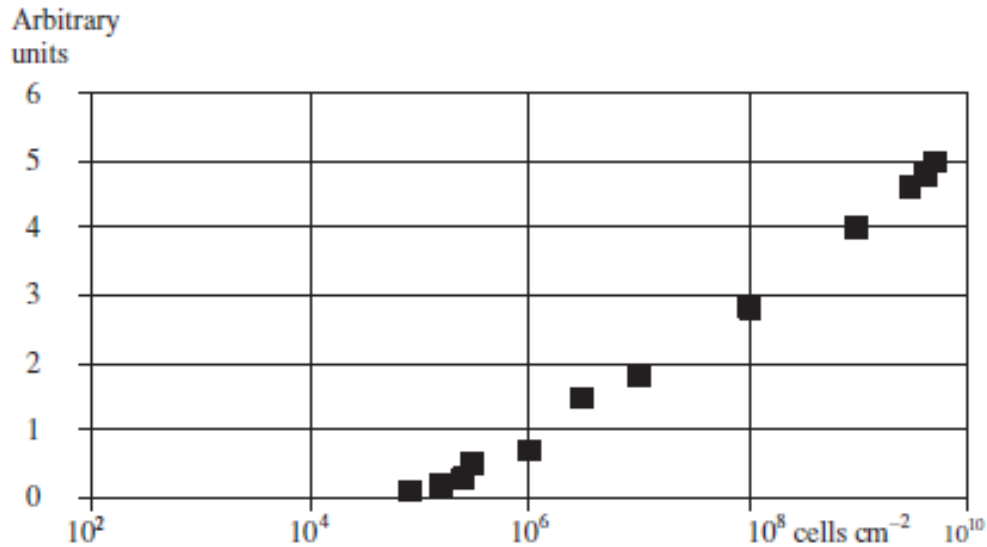
Figure 8. The intensity of the signal of backscattered light and surface cell density [9][8].

2.3.9 Optical Microscopy

Optical microscopy is the one of the most common and direct techniques used by researchers to identify microorganisms. Images of microorganisms have always been critical to understanding microbial characteristics, particularly those that occur on the surface. Microorganism growth can be quantified by greyscale or black & white analysis of images captured with a digital camera. Counting the percentage of white versus black pixels over a test area allows the calculation of microorganism growth on a surface [59]. This is a much simpler procedure compared to other methods (e.g. SEM or fluorescence) that require an extensive staining and preparation process (and which cannot be done online). The traditional microscope works well on early-stage biofilm growth as the light microscope requires visible light to be transmitted

---

[8] Figure reproduced with permission.

34

through the sample. However, as biofilm grow, the deposited biomass can block the light completely, resulting in a totally dark image. Furthermore, traditional microscopes can only provide 2D images, and as the biofilm thickens, the differing biofilm layers can interfere with image collection and processing.

To observe the surface at a larger and finer scale, confocal laser scanning microscopy (CLSM) can be used to provide both morphology and the depth profile of the biofilm surface. CLSM has a similar working principle as Optical coherence tomography OCT but uses a shorter wavelength as the light source in the visible spectrum (visible light) and collects images with a camera rather than collecting light with a photodiode. With the method, images are collected that show the morphology at the surface. By the movement of the focal plane, detailed 2D images can be collected and used to construct 3D images (by relying on the observation that out of focus details are blurred). In comparison with OCT, CSLM will have less penetration depth but higher resolution due to the shorter visible light wavelength [60].

2.3.10 Nuclear Magnetic Resonance Spectroscopy

Nuclear Magnetic Resonance (NMR) can be used to measure biofilm activity by characterizing metabolic products of microorganisms. The metabolism product concentration can be measured by detecting the concentration of the nuclei in the atoms. In NMR, the nuclei of these atoms will resonate under a certain frequency in a magnetic field (i.e. will be excited by an impulse of radiofrequency radiation). It is somewhat similar to the absorption and emission of radiation by electrons as described in the fluorescence section. Not all nuclei are NMR visible, however. In theory, nuclei that have an odd mass number or an odd atomic number has a nuclear spin. Typical

NMR visible nuclei include 1H, 13C, 15N, 23Na and 35Cl. There are two types of spin quantum number for NMR visible: 1/2 and quadruple nuclei. Biologically related spin ½ nuclei are 1H, 13C, 15N, 19F and 31P, quadruple nuclei are 14N, 23Na, 35Cl and 39K. Generally, the interpretation of the concentration of spin ½ nuclei is easier than the quadruple nuclei due to the complex energy transit of quadruple spin nuclei.

Each NMR visible nuclei resonate at its own frequency so-called Larmor frequency which under different setup, the Larmor frequency will vary as shown in Equation 15:

$$Vi = \gamma i * Bo \qquad (15)$$

where Vi is the Larmor frequency of the nuclei, γi is the magnetogyric constant of the nuclei and the Bo is the field strength of the NMR magnet [61]. However, due to different conditions and interactions, the actual resonate frequency will usually shift several MHz. Thus, a spectrum with a shift in frequency and magnetic field strength could be constructed. The sensitivity of the NMR, signal to noise ratio (S/N ratio) is related to nuclei concentration as shown in Equation 16 [61]:

$$S/N \propto C * Ns0.5 \qquad (16)$$

where C is the concentration of the nuclei and Ns is the number of scans. The NMR method can also be used to construct the morphology of the biofilm via the Magnetic Resonance Imaging (MRI) method [62]. It is rare that this method is applied outside of the laboratory, primarily due to the cost and difficulty of the set-up. However, lab test has been conducted in-situ using this method [63], but it takes a very long time (days) to collect an accurate spectrum [64].

2.3.11 Electrochemical method

The general approach of electrochemical methods is to monitor biofilm growth by applying and collecting electrochemical measurements. These methods typically apply constant current or voltage, either as an input or output. The change in the output value, current, voltage, and resistance (V/I) is observed. The setup of the reaction cell usually consists of a working electrode, reference electrode and a counter electrode. The increase of bacteria growth is reflected as an increasing larger current being needed to maintain a constant voltage value across the cell [65].

For example, cathodic current density, i(E,t), can be measured over time on a stainless steel sample in natural seawater solution and polarized at a constant potential E, and is described by Equation 17:

$$i(E,t) = i_1(E) + [i_2(E,t) - i_1(E,t)] * \theta(t) \tag{17}$$

where i_1 is the current density measured on the un-fouled surface of the stainless-steel sample under a given potential E and i_2 is the current density measured on the surface covered by θ (0 to 1) fraction of the surface under a given potential E. The change of I versus E will also describe different biofilm coverage. It can represent the intermediate process during the biofilm growth via potentiostatic (constant voltage) and intensiotatic (constant current) methods, respectively. Generally, the electrochemical method is done with stainless/carbon steel or noble metal as the working electrode and noble metal (Zn, Pt) as counter/reference electrodes. The Intensiotatic approach has higher sensitivity and can operate under $1\mu A/cm^2$. Detection sensitive for biofilm coverage by potentiostatic is around 1% cover of biofilm through an ALVIM sensor [66].

One of the advantages of electrochemical methods in practice is its current use in the corrosion industry. Electrochemical methods have been used to study traditional corrosion mechanisms for decades and is used to provide relatively accurate information on corrosion rate, corrosion current density, and other useful parameters [67] [68]. By combining the biofilm monitoring probe with the traditional corrosion monitoring probe, it may provide a viable way to distinguish traditional corrosion or MIC compare to other methods which only monitor biofilm activities.

The idea of applying electrochemical methods to detect bacteria and monitor biofilm activity has been examined in previous studies. This has included the measurement of both conductivity of the solution containing microbes [15] [69] and capacitance [16] [70] using dielectric sensors. For conductivity, the premise is that changes in the electric signal on the surface of the electrode could be correlated with the concentration of the cells in the solution. For capacitance, the proposed mechanism is that bacteria cells act as capacitors or dielectric elements when an applied electric field is applied, resulting in the movement of ions on either side of the cell membrane. Therefore, the oppositely charged ions accumulate on either side of the cell, accumulating charge across the membrane [71].

A common variation of electrochemical analysis is Electrochemical Impedance Spectroscopy (EIS). EIS is based on the measurement of the impedance (resistance and reactance) characteristics of a surface and/or fluid by applying a small-amplitude AC signal over a range of frequencies. EIS can be done with 2, 3, or 4-electrode systems, with the simpler 2-electrode systems being suitable when the impedance of the sample is much greater than the electrode lead impedance [72]. When this is not the case, one or two reference electrodes are required. The 3-electrode EIS measurement system has a single reference electrode and is the

most commonly used configuration. For a 2-electrode cell, the counter and reference electrode are replaced with a single electrode (ie the counter electrode).

The measured impedance from these scans, including both the real and imaginary parts (i.e. resistance and reactance), are plotted using a Nyquist diagram which correlates reactance versus resistance for a series of frequencies. These vary widely, depending on the nature of the biofilm under test. For example, Duan et al [73] used EIS to study the corrosion behavior of an anaerobic biofilm with SRB bacteria on carbon steel in natural seawater over a seven-day period. It was observed that the measured impedance decreased overtime.

EIS testing is typically done over numerous repeated runs where the frequency of a small AC voltage is swept over a range of discrete frequencies. Over the course of time, the impedance changes as corrosion progresses, and a series of curves are collected. The curves are then fitted using an "equivalent circuit," where the electrical elements are selected to reflect the nature of the biofilm under study. These vary widely, and the best-fitted curves are found via an iterative process. Further, the equivalent circuit will vary depending on the biofilm under study, with different equivalent circuits, for example, being suitable for IRB versus SRB.

An example of an equivalent circuit for corrosion of 316 SS by SRB is shown in Figure 9. The "R" factors are the resistance. "Q" factors are known as constant phase elements (CPE's) that account for the alteration in behaviour between actual and theoretical capacitance.
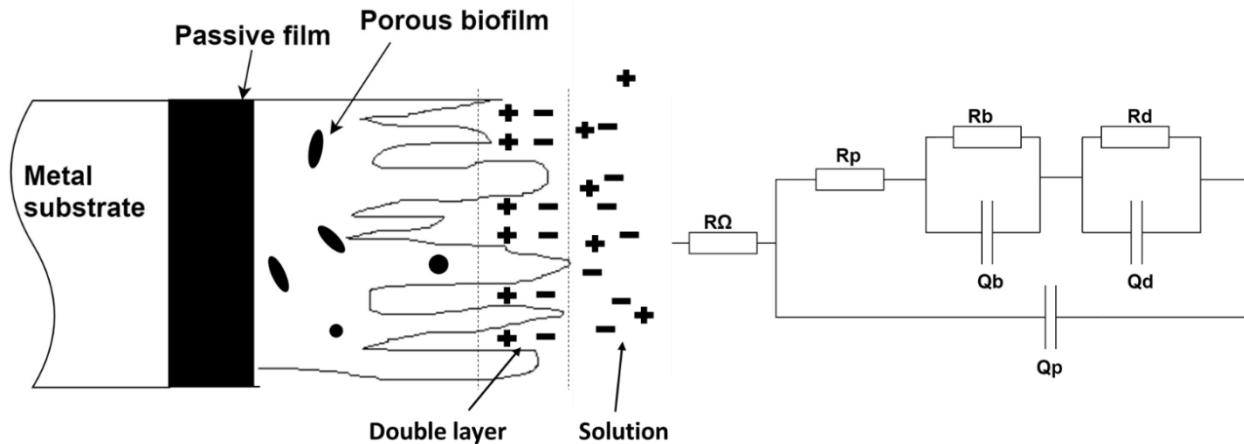
Figure 9. EIS Equivalent Circuit for a passive porous Biofilm adopted from [74]

In this example, $R\Omega$ is the electrolyte resistance; R_p and Q_p are the passive film resistance and capacitance; R_b and Q_b are the porous biofilm resistance and capacitance; R_d represents diffusion path length in the double layer, and Q_d is the diffusion of the charge carriers in the double layer. The "+" and "−" are positive and negative ions.

The EIS analysis is based on finding component values in the equivalent circuit that fit the data points recorded in the Nyquist plot. Observation of the trends for these derived component values is then related to the observed corrosion of the test coupon. Additional details, including variants of the equivalent circuits, comparisons with sterile media without SRB, comparisons between the passive and biofilms are available in the literature [75].

3. METHODOLOGY

3.1 Selection & Culturing of Model Bacteria Strain

In this study, *Pesudomonas putida* was used as the test microorganism, and was selected due to its ability to grow rapidly into a biofilm (grows in 2~3 days compared to traditional SRBs which take weeks). This microorganism is also commonly found in produced water and sludge. It has also been reported to have some corrosion effects on steel surfaces, however, the mechanism is not fully understood [76, 77]. In this study, *Pseudomonas putida* (an aerobic, gram-negative bacteria strain) was isolated from the known MIC sludge, and was identified using 16s RNA sequencing [78]. To perform the sequencing to final identify the strains, DNA extraction and Polymerase chain reaction (PCR) were first performed [79].

A Qiagen DNA ease kit was used to extract the DNA from the strain. The isolated colonies were first cultured overnight in LB broth (to grow enough bacteria) and then was placed in a centrifuge (spun-down) to obtain the required number of cells (approximately $2x10^9$ cells). The DNA extraction process was divided into two steps: a) Lysis of cells and b) DNA purification. Lysis of cells was sued to break down the cells into components (including DNA segments) which are collected through DNA purification. To perform lysis of cells, 180µl enzymatic lysis buffer was added into 20 µl concentrated cells and then incubated at 37ºC for at least 30 min. After incubation, 25 µl proteinase K and 200 µl Buffer AL (contains HCl and NaCl) was added and mixed, followed by incubation at 56ºC for 30 min to ensure the lysis of the proteins within the cells. Finally, 200 µl 100% ethanol was added to precipitate the proteins. After the lysis of cells steps, DNA extraction was performed by placing the mixture into a mini spin column inside a collection tube, then centrifuged at >6000 g for 1 min. This process was repeated twice using a

washing buffer, and centrifuging at 6000 g and 20,000 g for 1 min and 3 min, respectively. These latter steps were performed to ensure the removal of all ethanol as it can interfere with subsequent reactions. Finally, the DNA was eluted from the spin-column by adding elute buffer followed by an incubation at room temperature for 1 min and then centrifuging at > 6000 g. The concentration and purity of the DNA was determined using a spectrophotometer (NanoDrop One, Thermofisher). It applies the Beer-Lambert law to convert Optical Density (OD) to the concentration of DNA in ng/µl. The Optical Density is calculated using equation 18:

$$OD= Log(\frac{Intensity \ of \ incident \ light}{Intensity \ of \ transmitted \ light})$$ (18)

In this study, the wavelength used in the spectrophotometer to determine the concentration of the DNA was 260 nm (A260). In this case, the DNA extracted from the cells were single-stranded DNA (ssDNA). As such, 1 OD value (A260) was equal to a DNA concentration of 33 ng/µl. The purity and quality of the DNA was verified by applying additional optical densities using two different incident light wavelengths: 230 nm (A230) and 280 nm (A280). The ratio of A260 to A280 determines the nucleic acid contamination in protein (the ratio should be around 1.8 to considered as "pure" DNA with <25% protein), while the ratio of A260 to A230 can determine the protein contamination in nucleic acids (the ratio should be larger than 2.0 to considered "pure").

Polymerase chain reaction (PCR) is a technique commonly used to copy specific pieces of DNA through a heat process. First, a mixture was prepared with a master mix (including dNTPs, thermostable polymerase), primers and DNA. The primer used in this process was 16s primer (8F,1492R) with a sequence of AGAGTTTGATCCTGGCTCAG (forward) and ACGGCTACCTTGTTACGACTT (reverse). The forward and reverse primers allow the copy of

the DNA from both forward and reverse directions for the double strand of the DNA. The mixture composition of the PCR was shown in Table 2:

Table 2. The composition of the PCR mixture per tube. (25 µL system)

Reagent	Volume(µL)
Green master mix	12.5
Forward primer(10mM)	0.5
Reverse primer(10mM)	0.5
Nuclease-Free water	Balance
DNA template	50ng depends on the concentration
Total volume	25

For each PCR reaction test, there is a negative control needed in order to confirm the validity of the reaction. For negative control, nuclease-free water was added instead of the DNA template. After mixing the samples, they were then briefly centrifuged to ensure all the reagents were mixed on the bottom. The tubes were then placed in the PCR machine (Mastercycler, Eppendorf), and amplification parameters were selected based on the primers used and the length of the sample DNA. The thermocycle for these analyses is provided in Table 3:

Table 3. Thermocycle of PCR reaction (16s Primer)

Stage	Temperature(ºC)	Duration	
Initial denaturation	94	5min	
Denaturation	94	45s	
Annealing	58	45s	Repeat 30X
Extension	72	90s	
Final Extension	72	7min	
Hold	4	∞	

The process of denaturation to extension was repeated 30 times to generate sufficient copies.

Gel electrophoresis was then performed to verify the success of the PCR reaction by determining the lengths of the DNA generated. This was accomplished by pipetting 5 µL of the PCR product into the wells on the pre-made gel along with DNA ladder (to determine the length of the DNA) and a negative control. These were then immersed in Tris/Borate/EDTA (TBE) buffer, and a current of 400 mA (under 150 V) was applied for 40 min to allow the nucleic acid to travel upwards. The resulting procedure was found to verify the success of the PCR reaction as shown by the image of the gel under X-ray in Figure 10. In this figure, the negative control shows no sign on the graph, and the two samples have the same DNA length at around 800 bp (base pairs).

Prior to sequencing, the DNA was separated and cleaned from the PCR mixture using GeneJET Gel Extraction kit. Next, the PCR mixture on the purification column was collected and added to 100 µL of binding buffer. This was then centrifuged at >6000 g for 1 min to bind the DNA product to a separation column. Then the flow-through was discarded, and 700 µL of wash buffer was added and centrifuged at >6000g for 2 min to wash off any contaminants and the residual buffer. Finally, 50 µL of elution buffer was added to elute the purified DNA into a new, clean 1.5 ml tube. Using the Nanodrop machine, the concentration and purity of the recovered DNA was verified, and a mixture for sequencing was prepared.

Finally, Sanger Sequencing was performed on the purified DNA in order to obtain the sequence. Two sequences were obtained: one is the front sequence and the other is the reversed one. The sequences from first non N character to the last character before N was copied, and was compared to the NCBI database (National Center for Biotechnology Information, Maryland USA) to confirm the identity of the strain. After confirmation, the strain was stored as a stock culture by mixing the overnight culture with 70% glycerol, and then transferred to a freezer at -80ºC. Samples were withdrawn, as required, and used for subsequent testing.

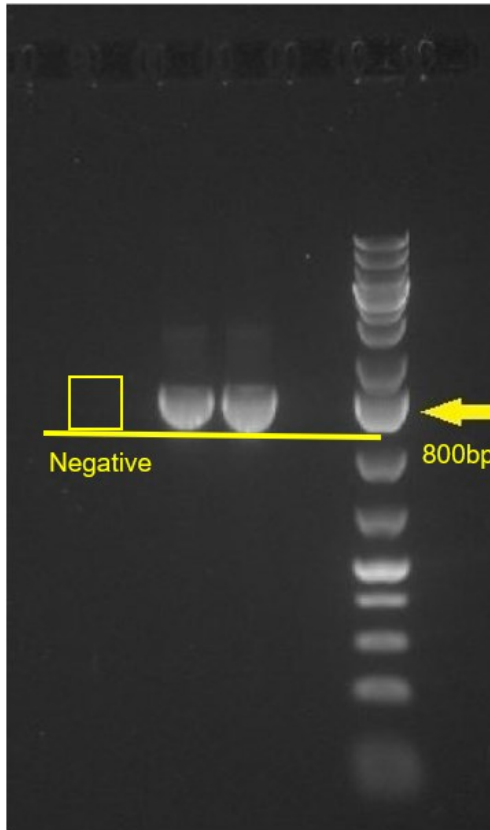**Figure 10. Gel result from the PCR reaction of *P.putida***

3.2 Overview of the Testing Probes

3.2.1 Parallel Plate System

The parallel plate probe system is a two-electrode system fabricated using two 316 stainless steel plates stacked face to face and separated by a predefined distance (gap size). This configuration allows the characterization of total bacteria in the gap between the plates, including

suspended bacteria in solution (i.e. planktonic bacteria) and bacteria cells aggregated on the plate surfaces (i.e. sessile bacteria).

In this study, each electrode was fabricated by first taping a copper wire to the stainless-steel plate then embedding the assembly in 2-parts epoxy using a removable cylindrical mold. A customized clamping system was developed to hold the two electrode assemblies in place and to ensure a uniform and precise gap between the exposed plates.

The clamping system consists of two Polyether Ether Ketone (PEEK) clamping plates, three bolts with nuts, and PEEK washers to adjust the gap between plates (electrodes). The PEEK clamping plates were waterjet cut to make a ring-like shape with three nodes to hold the bolts in place (see Figure 11). The bolts were used to connect the two electrodes face to face in place, as shown in Figure 12.
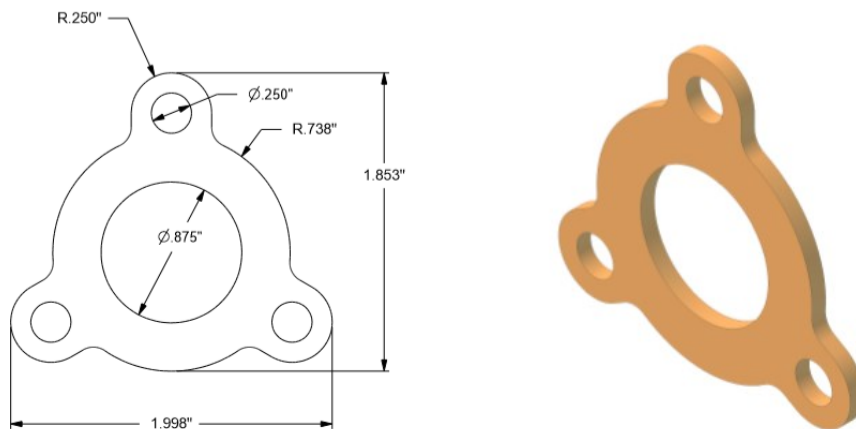
Figure 11. Dimensions and rendering of the clamping plate.
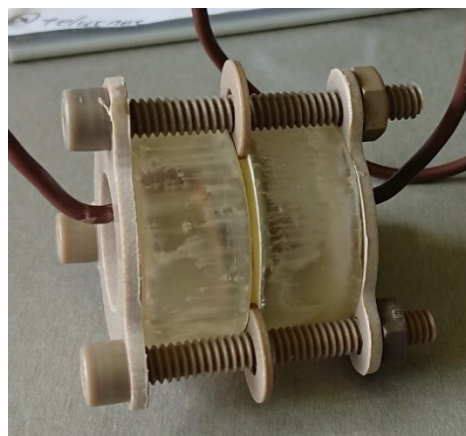
Figure 12. Photo of the assembled parallel plate system.

3.2.2 Interdigitated Electrodes (IDE)

Interdigitated Electrode (IDE) microchips were procured from Metrohm AG Instruments (USA). Each IDE chip consists of two inter-dispersed metallic strips (fingers) deposited on a thin glass substrate, as shown in Figure 13. These thin metallic strips are separated from each other by a fixed gap size and are attached to larger metallic pads that can be connected to a measuring device.

In this study, preliminary tests were performed on IDEs made from two available metal types, gold (Au) and platinum (Pt), and with two different gap sizes, 5 μm and 10 μm. The overall dimensions of these chips were 22.8 mm L x 7.6 mm W x 0.7 mm H, and the thickness of each metallic strip was 5nm. Prior to testing, each IDE micro-chip was initially cleaned in two steps by immersing it in boiling Acetone solution for 1 min followed by immersion in a boiling Trichloroethylene (TCE) solution for another minute. After cleaning, the chips were then immersed in 70% ethanol and sonicated for 1 min, rinsed, and dried to eliminate any excess solvent.

While the previous parallel plate system measures total bacteria counts (sessile and planktonic), the IDE system was used to try to quantify both total bacteria count (sessile and planktonic), and bacteria counts deposited as an attached biofilm (sessile only). This was accomplished by using two separate testing procedures as outline in Sections 3.3.2 and 3.3.3.
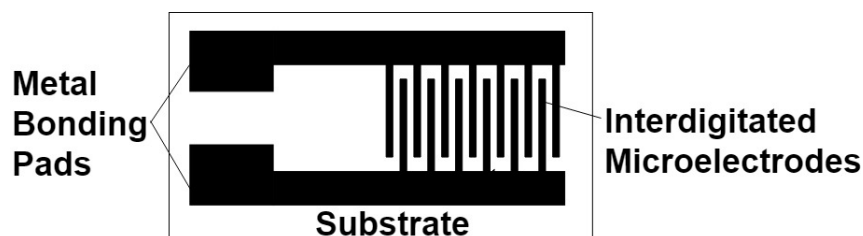
Figure 13. Schematic of an Interdigitated Electrode (IDE) microchip.

3.3 Testing Procedures

3.3.1 Parallel Plate Testing

Before each test, each electrode plate surfaces were ground with a variety of grit paper sizes (starting at 240 grit up to 600 grit), and then cleaned with 70% ethanol between each run. A PortHoles™ mask with a circular cutout (Gamry Instruments) was applied to the surface of each electrode to restrict the exposed area. Within 1 hour after grinding and application of the mask, the electrodes were assembled by putting the clamping plate into the bolt and tightened with nuts. A filler gauge was used to ensure the gap size between electrodes was met. The assembled probe was immersed completely into 70% Ethanol for 10 minutes and let dry. After sterilization, the device was then transferred into a 1-litre glass reactor filled with 0.9% NaCl solution. The electrodes were then connected to a potentiostat (Gamry Reference 600 System) and associated computer for data

logging. This setup is shown schematically in Figure 11. Since this setup is essentially a 2-electrode system, the reference electrode input was connected directly to the counter electrode input. The entire glass reactor was then put in a shaker water bath at 30°C and 50 RPM to ensure the suspension of the bacterial cells. Prior to introducing bacteria, however, the system was run for at least 20 hours to stabilize and collect EIS baseline readings. Data was then plotted using Zview software (Scribner).

To obtain sufficient bacteria for the parallel plate tests, withdrawn samples were further cultivated aerobically for 24 hours in a Lysogeny broth (LB) medium using an incubator shaker (Innova 44, New Brunswick Scientific) at 30°C and 200 RPM. The overnight culture was then centrifuged at 5,000 RPM for 10 minutes using an Allegra 25R centrifuge (Beckman Coulter). From this, the supernatant was discarded, and the bacteria concentrate was re-suspended in 10 ml of 0.9% NaCl buffer solution. The number of cells in the solution (CFU/ml) was quantified using both optical density (OD) measurements at λ=600 nm (Ultrospec 100 Pro, Biochem) and spread plating through serial dilution. In order to ensure a consistent bacterial concentration, the solution was adjusted to achieve an optical density measurement of 0.2 abs (approximately 9.3×10^8 CFU/ml). This solution was used as the feedstock for performing tests with the parallel plate system, as outlined in the next section.

To measure the effect of bacteria concentration on the resulting EIS measurements, the bacterial cell concentration in the test reactor was incrementally increased by adding a fixed volume of suspended cells in solution in a 10-fold manner: 1μL, 10μL, 100μL, 1ml, 5ml and 10ml. This was injected into the reactor in a 20 min interval to ensure proper mixing and cell attachment. At each increment, an EIS sweep was collected using the potentiostat for a frequency range of 10 000 Hz to 0.1 Hz at 8 to 10 steps per frequency decade and voltage amplitude of 10 mV. EIS

measurements at each step are repeated at least twice (duplicate) to ensure consistency of the data. After each run, the spectrum collected was then fit to an equivalent electrical circuit, which is intended to model the electrode, the passive film (including any biofilm), and the solution between the metal plates. From this model, the effective capacitance of the system (including the presence of bacteria) was determined.

3.3.2 Interdigitated Electrode (IDE) Microchip Testing

Two separate test methodologies were performed in this study to assess the ability of Interdigitated Electrode (IDE) microchips to measure the presence and quantity of microorganisms in a fluid system using electrochemical techniques. The first methodology (denoted "sessile") measures the response of the IDEs to various concentrations of bacteria which are deposited on the surface of the IDE immersed in a growing culture. The second methodology (denoted "total bacteria") measures the response of the IDEs to various concentrations of total bacteria (including both planktonic and sessile) when the IDE is immersed in a fluid system with a known (fixed) bacteria concentration (similar to the method used in the parallel plate tests). Each are described in the following sections.

3.3.2.1 Testing of IDE Chips for Total Bacteria (Planktonic and Sessile)

Similar to the tests for the parallel plate sensors, the IDE chips were also tested to assess whether they can detect and quantify total bacteria counts (planktonic and sessile) in a solution. First, new IDE chips were cleaned with 70% ethanol, rinsed with DI water, and dried under nitrogen to prevent contamination. A stock culture with an optical density reading of 0.2 abs was prepared using the same procedure as described in 3.3.1. To test the EIS response under different

total bacteria concentrations, a dilution series was prepared by adding different volumes of stock solution to testing tubes containing 0.9% NaCl buffer. The resulting solutions had a range of bacteria concentrations ranging from 9.3×10^1 CFU/ml to 9.3×10^7 CFU/ml (incremented in a 10-fold manner). After the dilution series was prepared, the cleaned IDEs were then connected to the potentiostat via the adapter.

As shown in Figure 14, the interdigitated section of each IDE was then dipped into the prepared diluted solution with a specific bacteria concentration, and an EIS test was run using the settings described in section 3.3.1. For each IDE chip, the EIS test was performed three times to ensure the consistency of the result. After the EIS tests for one bacteria concentration was completed, the IDE was retracted from the adaptor and was cleaned with 70% ethanol, rinsed with DI water, and dried thoroughly under nitrogen. For each type of IDE chip, three replicates of the stock solution were also prepared and used to ensure biological replication. With the 3 EIS test replicates and 3 biological replicates, each IDE type (material and gap size) was tested for a total of 9 replicates to determine experimental variability.


Figure 14. The IDE setup for measuring total bacteria count (the IDE is immersed in buffer solution with different bacteria concentrations).

3.3.2.2 Testing of IDE Chips for Sessile Bacteria

For the sessile test methodology, experiments were conducted in a biosafety cabinet where a HEPA (High-Efficiency Particulate Air) filter to minimize contamination, as shown in Figure 15. Prior to each test, each IDE was sterilized by first rinsing with 70% ethanol, and then placed it into a petri dish containing enough 100% ethanol to immerse the IDE. The petri dish with the IDE was then left in the biosafety cabinet until all the ethanol was evaporated. After evaporation, the IDE was again immersed in 100% ethanol and left to dry. The sterilized IDE was then placed into a pre-sterilized vial with a sponge stopper. One colony of the *P.putida* strain (from the recovered stock culture) was placed into 10 ml Lysogeny broth (LB) medium, and then 1 mL of this inoculated medium was transferred to the test vial containing the IDE micro-chip. The sponge stopper was placed back on top to ensure aerobic conditions. Next, the vials were then incubated at 30°C for up to 4 days in a shaker incubator (Max Q400, Thermo scientific) at 200 RPM to grow the bacterial population and to ensure the deposition of bacteria cells on the surface of the IDE micro-chip. It was postulated that a longer immersion time would result in higher sessile bacteria attachment to the IDE surface.

The vials containing IDEs will stay in the incubator for up to 4 days. The adaptor for the IDEs was put on a rack and placed in the biosafety cabinet with the wires sticking out to connect the potentiostat on the cart beside the biosafety cabinet. An electric incinerator was also placed in the cabinet for sterilization of the tweezers. Sanitize the setup inside the biosafety cabinet by wiping down the rack and its accessories before every EIS test (Figure 15).
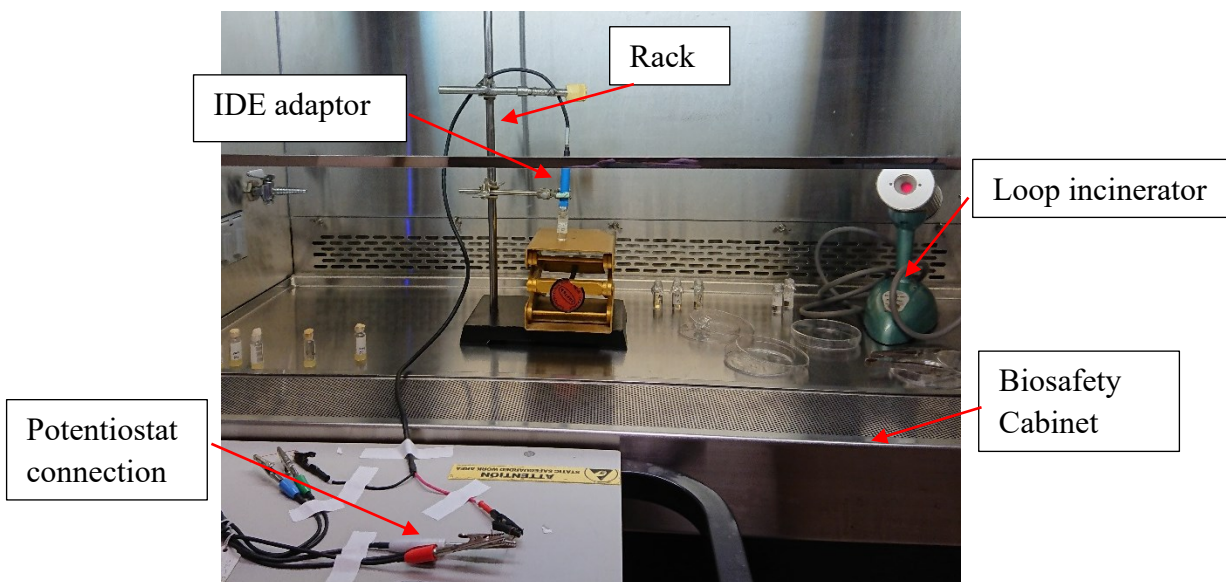
Figure 15. The Sessile IDE testing setup within the biosafety cabinet.

At predetermined time intervals, each IDE was removed from the growth medium and was carefully attached to a special adaptor connected to the potentiostat (located outside the biosafety cabinet). As shown in Figure 16, the interdigitated section of the removed IDE was then immersed in a vial containing 4.8 ml of 0.9% NaCl, and EIS measurements were then taken immediately using the same settings as noted in the previous section 3.3.1. After each EIS test, the metal bonding pads section (contact with the adaptor) was dipped into 70% ethanol and let dry to avoid cross-contamination. Next, the whole EIS micro-chip was immersed into the same vial containing 4.8 ml of 0.9% NaCl solution, and was then sonicated for 3 min at 42,000Hz using an ultrasonic cleaner (Sper scientific) to remove the bacteria cells from the IDE surface. 1 ml of this buffer solution containing the bacteria cells was then used to quantify the number of sessile cells on the IDE surface (in CFU/mL) by performing serial dilution and spread plating count method. This procedure was ultimately repeated several times using new IDE micro-chips

(sacrificial) over increasingly longer incubation times to generate a wide range of bacteria concentrations.
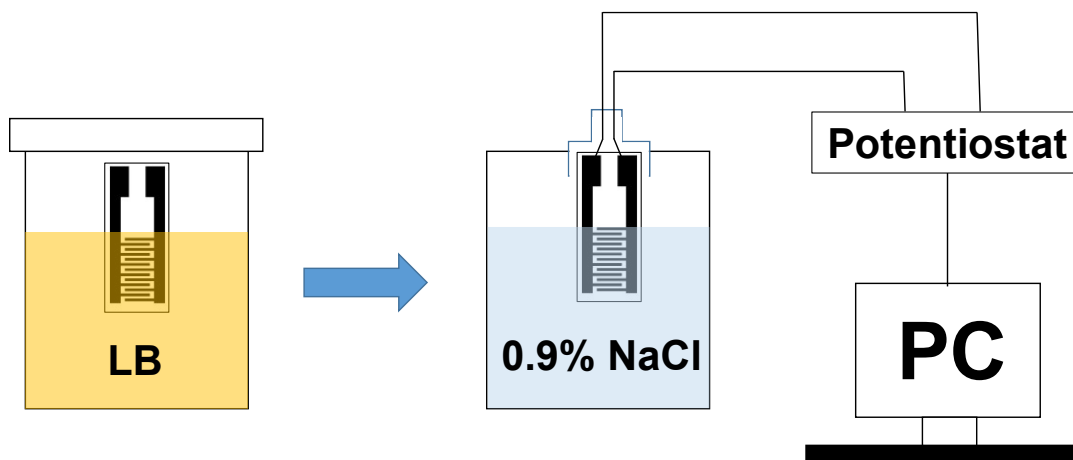
Figure 16. Schematic of the IDEs were removed from the culture medium and moved to a buffer to perform EIS testing.

3.4 Optical Microscopy

A limited number of samples after testing were assessed using optical microscopy. IDE chips with surface bacteria were placed on a microscope slide and were examined using a transmission microscope (Zeiss Axio Imager M1) at different magnifications (40X, 100X). Both still and video images were recorded.

4. EFFECT OF BACTERIA CELLS ON ELECTROCHEMICAL RESPONSE

4.1 Parallel Plate Probe Test Results

### 4.1.1 EIS Responses from the Parallel Plate Setup

The EIS response curves were plotted in the form of Nyquist and Bode diagram for the various parallel plate configurations, as shown in Figures 17 and 18, respectively. The Nyquist diagram (Figure 17) shows the changes in impedance values as a function of bacteria concentration for two different plate gap sizes (0.5 mm and 1 mm), and two plate surface area sizes (1 cm^2 and 2 cm^2). In these graphs, Z' is the real impedance value and Z'' is the imaginary impedance component. Bacteria cell concentrations tested ranged from 0 (control with no bacteria present) to approximately $9.3x10^9$ CFU/ml.

According to the Nyquist diagram pattern, a mass transfer process and diffusion process seem to co-exist as neither a semi-circle pattern nor a straight-line pattern, but a hybrid shape was observed. In general, it can be seen that the slope of the impedance curves decreases with increasing bacteria concentration. As the bacteria concentration increases, the difference between curves is quite small until approximately $9.3x10^8$ CFU/ml, where there is a noticeable drop in slope. This is observed to occur for all gaps and surface area combinations tested. This threshold value likely represents the critical point where increased bacteria concentration results in the formation of an aggregate of cells on the inner plate surfaces of the probe.

Beyond this concentration, the slope of these curves continues to drop until it reaches a minimum value of approximately 7.4×10^9 to 1×10^{10} CFU/ml (likely corresponding to a saturation point). Unfortunately, our test method was unable to distinguish between the contributions of the planktonic and sessile bacteria to the overall measured impedance values as the status of the bacteria between the electrodes cannot be directly observed.

In terms of gap size effects, there seems to be slightly better sensitivity (differentiation in slope) at low bacteria concentrations for the probes with a 0.5 mm gap size (versus the 1 mm gap size). This could be due to a preferential attachment of bacteria to the inner plate surfaces in a smaller gap.

The Bode diagram derived from basic EIS measurements are shown in Figure 18. These plots show the changes in the magnitude of impedance and phase angle versus the applied frequency values for various bacteria concentrations. Overall, the Bode diagrams support the observations found in the Nyquist plots. As bacteria concentration increases, there is a drop in both the impedance magnitude and phase angle for all frequencies considered. Tests with the 0.5 mm gap size tended to have a more distinguishable pattern compare to the group with the 1 mm gap size as the gaps between different bacteria concentration is more significant.
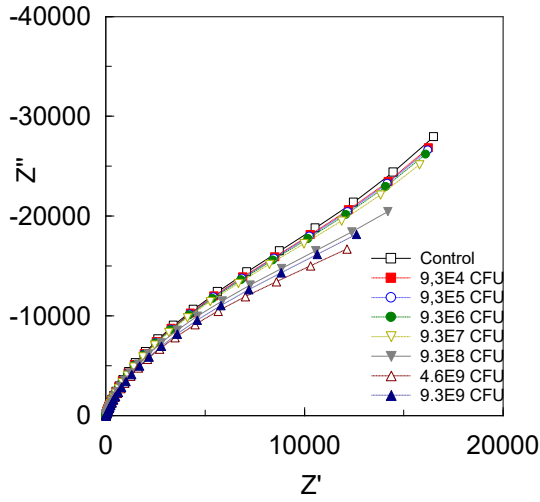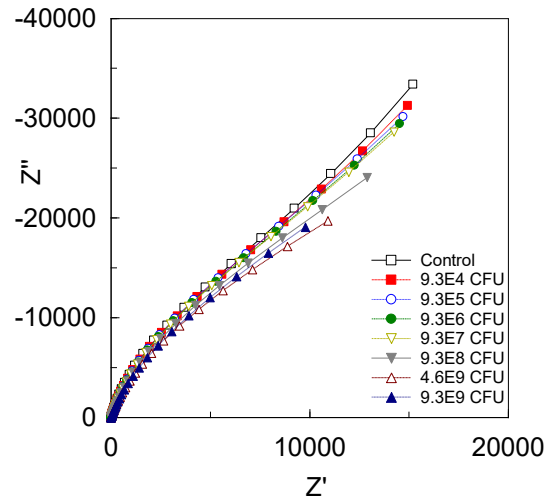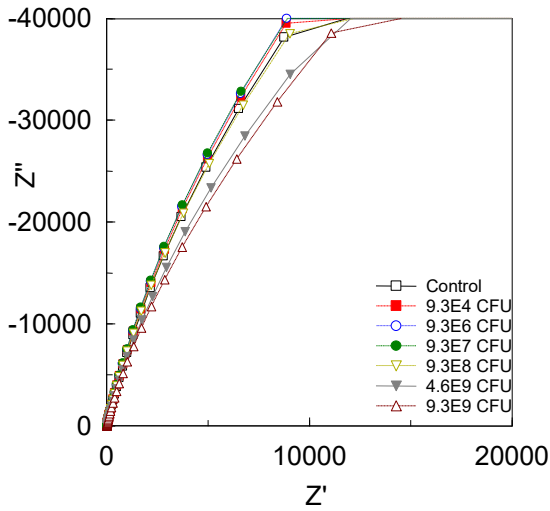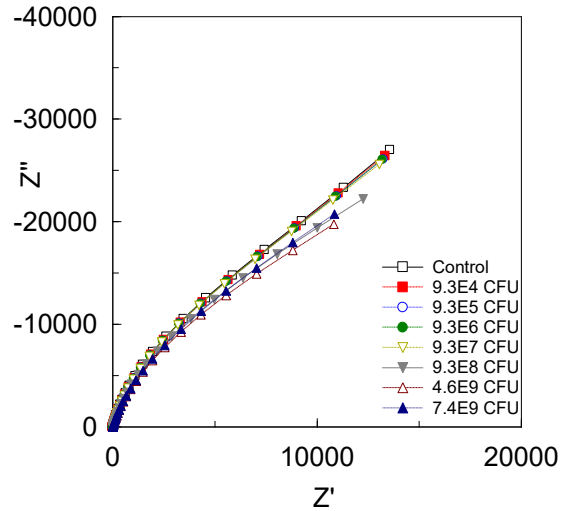
Figure 17. Nyquist diagram collected A) from EIS with 0.5mm gap size and 1cm² surface area. B) 0.5mm gap size and 2cm² surface area. C) With 1mm gap size and 1cm2 surface area and D) 1mm gap size and 2cm² surface area.
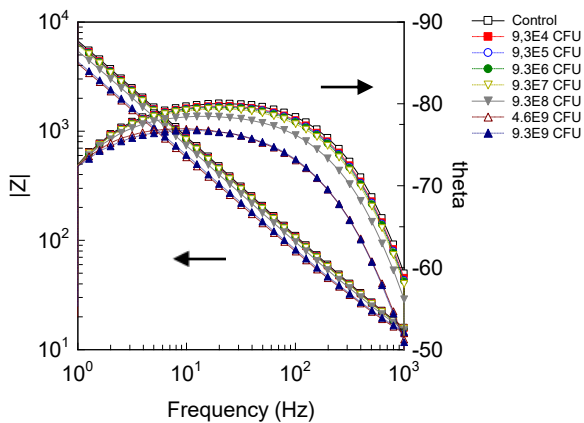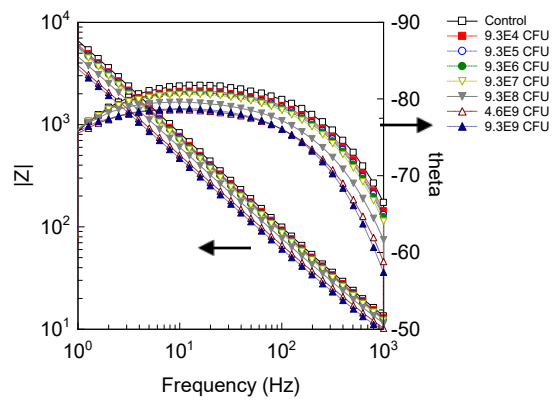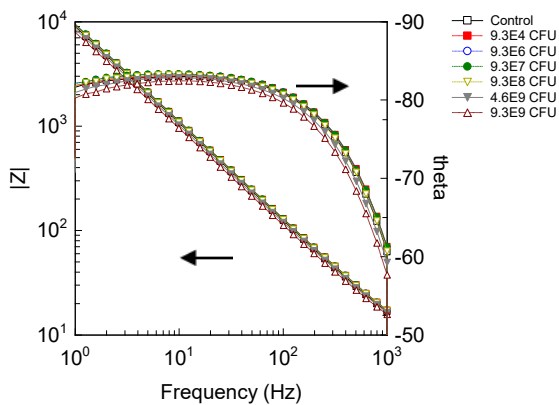
Figure 18. Bode diagram collected A) from EIS with a 0.5mm gap size and 1cm² surface area. B) 0.5mm gap size and 2cm² surface area. C) With 1mm gap size and 1cm² surface area and D) 1mm gap size and 2cm² surface area.

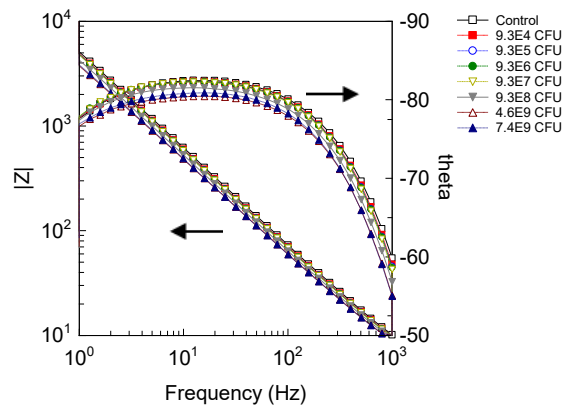## 4.1.2 Interpreting the EIS Data for the Parallel Plate Setup

While the general trends and patterns observed from the Nyquist and Bode diagrams provide some insight into sensor performance and biofilm formation, it is crucial to further study the measured EIS response in a more direct and quantitative way and to understand the nature of the interface between the electrodes and the solution that contains bacteria cells. In EIS analysis, the raw data on the Nyquist and Bode diagram is often fit to an "equivalent electric circuit." In this method, electric circuit elements (such as resistors and capacitors) are selected to reflect the nature of the interface under study. These can vary widely, and the best-fit model elements are often found via an iterative process.

In this study, an equivalent circuit was constructed based on the nature of the interface and was modified from Gonzalez et al [75]. The accuracy of the equivalent circuit was validated by the Chi^2 of the fitted curve compared to the data point with reasonable assumptions. The fitting process was done by Gamry Echem analyst software. It is proved that this equivalent circuit has a $Chi^2 < 0.0004$, which was considered a good simulation. The equivalent circuit constructed, which models the electrode, the passive layer/biofilm, and the solution between the metal plates and their relevant position in the system, as shown in Figure 19.
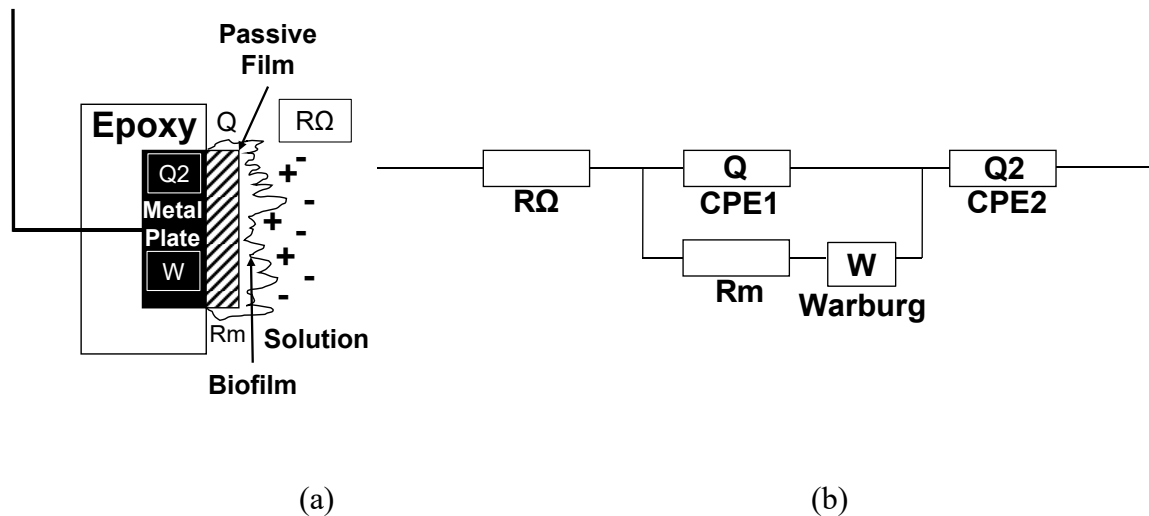
Figure 19. Equivalent circuit model used to evaluate the electrochemical response derived from EIS: (a) schematic of an electrode plate, and (b) electric circuit elements (RΩ, Rm is the resistance of the solution, passive film respectively; CPE1 and CPE2 is the constant phase element of the passive film and metal, respectively; W is the "Warburg Element").

As the circuit diagram and the schematic suggest, RΩ represents the resistance of the solution, and it is the first segment of the interface. RΩ is then connected in parallel with constant phase element (CPE1), Rm and the Warburg element. Rm is the resistance of the passivefilm, and CPE1 and CPE2 are constant phase elements that can act as a resistor and capacitor at the same time depending on a fitting constant α. If α=1, then CPE is an ideal capacitor, and if α=0, the CPE is an ideal resistor. It should be noted that the constant phase elements (CPE1 and CPE2) were introduced due to the two electrode configuration of this setup which is a non-ideal case (as charge transfer and diffusion can take place at the same time). Finally, the Warburg element (W) is used

to accommodate the diffusion process. The best fit values for CPE1 and CPE2 in this study were found to be between 0.8 and 1, suggesting that these elements behave mainly as capacitors. As such, CPE1 is reported in subsequent figures as an "effective capacitance" based on the output of the circuit element. In general, CPE1 and Rm could be considered the capacitance and resistance of the combined metallic passive film and biofilm layers for the probes being considered. Meanwhile, the CPE2 value can be seen as the capacitance of the interface between the bulk metal and the oxide/biofilm layer. As such, the resistance (Rm) and effective capacitance values (CPE1) derived from fitting the EIS experimental results to the model circuit were determined for both the parallel plate and IDE probe systems.
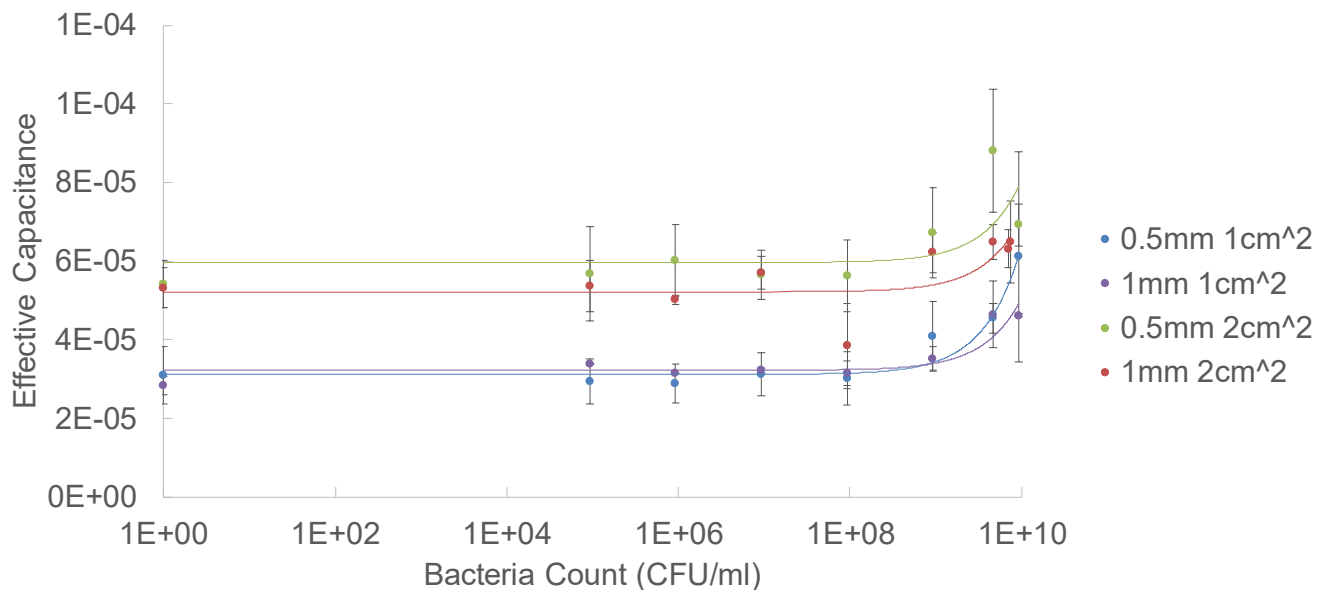
The effective capacitance of the parallel plate setup as a function of the bacteria concentration (planktonic and sessile combined) is shown in Figure 20 for each gap size and surface area combination. The trend lines provided on this graph represent the best fits of each data set. Overall, it can be seen that the effective capacitance for all configurations remains constant until a threshold value of approximately 10^8 CFU/ml is reached. This result is identical to that shown by the Nyquist diagram in Figure 17 as the significant change of slope can be found around 10^8 CFU/ml. This effective capacitance value, however, does a much better job of explaining the underlying physics of the observations and supports the theory that this concentration threshold represents the formation of the aggregate of cells on the inner plate surfaces of the probe. Furthermore, the results demonstrate that this approach may provide a valid method to detect aggregation cells in fluid systems.

In terms of the differences between the parallel probe options, Figure 20 shows that the probe surface area has a bigger effect on capacitance than the gap size between the plates. In fact, the effective capacitance of the probe with the larger plates (2 cm^2) is approximately twice the

capacitance of the smaller plate probe (1 cm^2). This is expected based on the theoretical formula

for a parallel plate capacitor, as shown in Equation 19:

$$C = \frac{\varepsilon A}{d} \qquad (19)$$

where C is the capacitance between the parallel plates, A is the area of the plate, d is the

distance between plates, and ε is the dielectric constant. While this formula is seen to predict the

effect of plate surface area in our tests, it does not accurately predict the effect of gap size which

saw a minimal change in effective capacitance. As a result, the baseline capacitance readings for

each case can therefore be attributed to the overall surface area of the probe and the characteristic

protective layer of the substrate material.

Figure 20. Change in effective capacitance with increasing total bacteria concentration for various parallel plate configurations tested (probe gap size in mm, and surface area in cm^2).

62

In addition to the effective capacitance (CPE1), the behavior of other elements of the model circuit were also examined. As shown in Figure 21, the resistance of the solution ($R\Omega$) and the passive/biofilm (Rm) are both seen to be relatively insensitive to bacteria concentration (constant). These results suggest that such measures are ineffective at detecting the presence of microorganisms. For the solution resistance ($R\Omega$), it can also be seen that a smaller gap size between plates results in a lower resistance. This is likely due to the lower volume of solution between the plates resulting in a decrease in the measured resistance. The resistance value of the passive layer (Rm) is also much greater than the solution resistance ($R\Omega$). This is probably due to the higher resistances associated with the dense oxide layers formed on the surface of the stainless-steel plates compared to the resistance of solution [80].
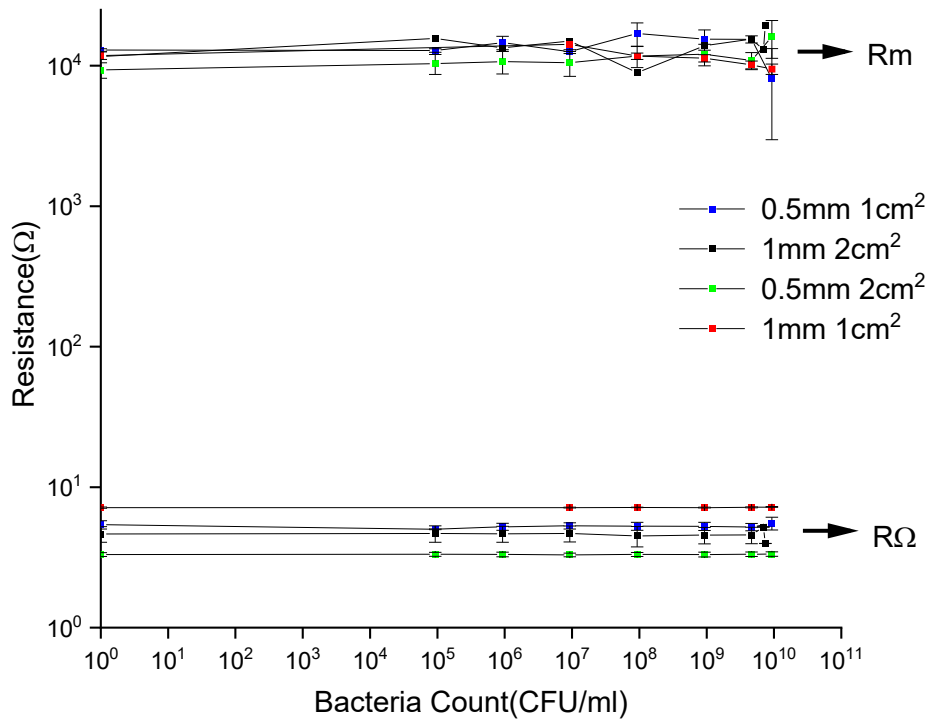

Figure 21. Changes in passive Film Resistance (Rm) and Solution Resistance ($R\Omega$) with increasing total bacteria concentration for various parallel plate configurations tested (probe gap size in mm, and surface area in cm².).

4.2 IDE Test Results (Total Bacteria Method)

## 4.2.1 EIS Responses from the IDE Testing (Total Bacteria Method)

The EIS data collected for the IDE microchip test using total bacteria methodology was plotted in the form of Nyquist and Bode diagrams, as shown in Figures 22 and 23, respectively. Response curves were plotted for two IDE materials (gold, platinum) and two gap sizes (5 µm, 10 µm). Bacteria cell concentrations ranged from 0 (control with no bacteria present) to approximately 9.3×10^7 CFU/ml. The Nyquist diagram shows that variation between IDE options are distinguishable and repeatable. However, the trends for the various conditions, unfortunately, are not consistent among the various options tested (i.e. material type and gap size). From a theoretical perspective, the mass transfer and diffusion mechanism seem to co-exist except for the gold 5 µm group. The Nyquist pattern for the other three groups is a hybrid shape (circle and straight line) which suggests a process that is more diffusion related. For the gold 5µm IDEs, all of its Nyquist response is a semi-circle shape suggesting a charge transfer process. In general, the impedance curve increases as the bacteria concentration increase for the gold material IDEs, similar to the parallel plate probes. However, the impedance curve for the Platinum material IDEs do the opposite (decreasing impedance with increasing bacteria concentration).
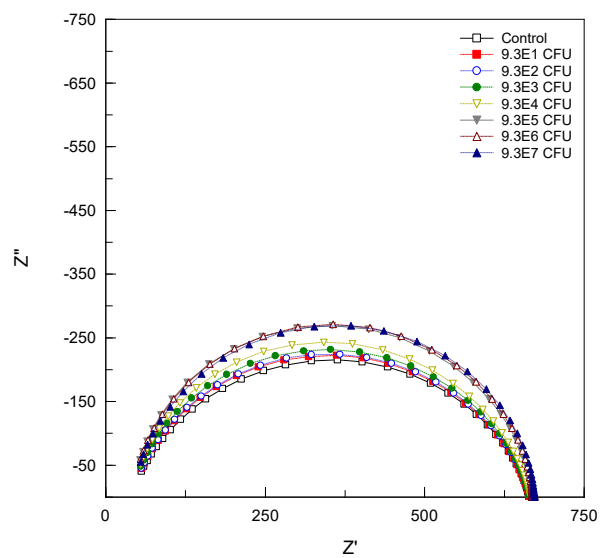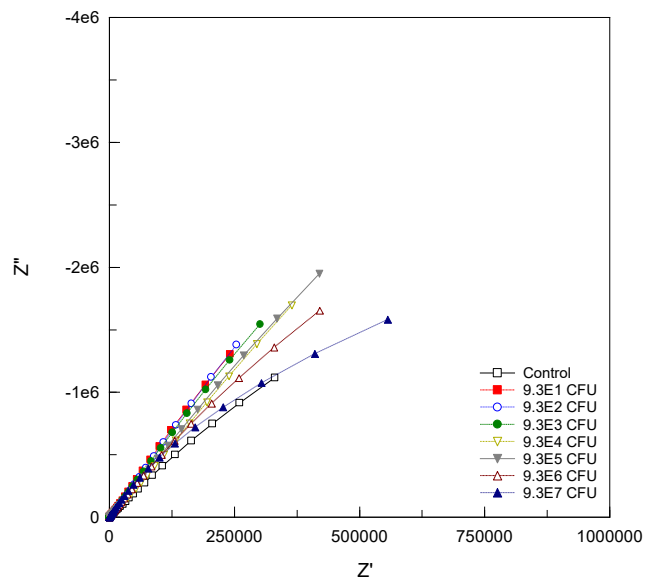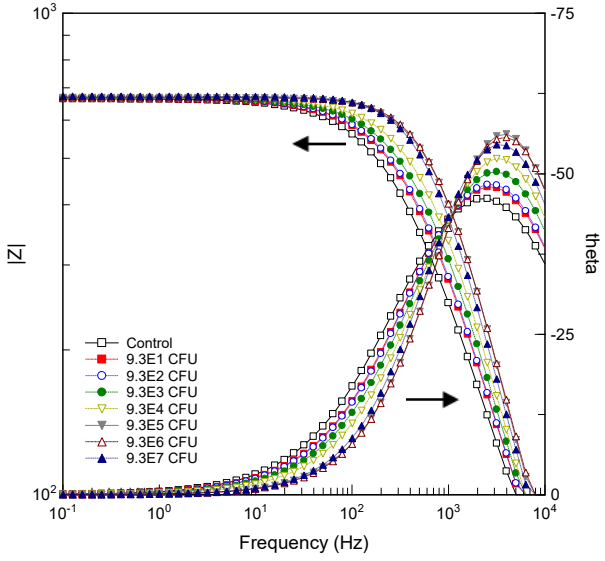
(a)
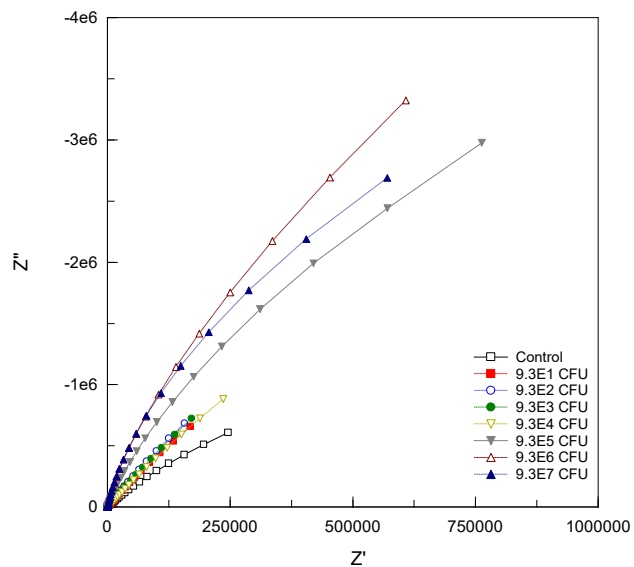
(b)
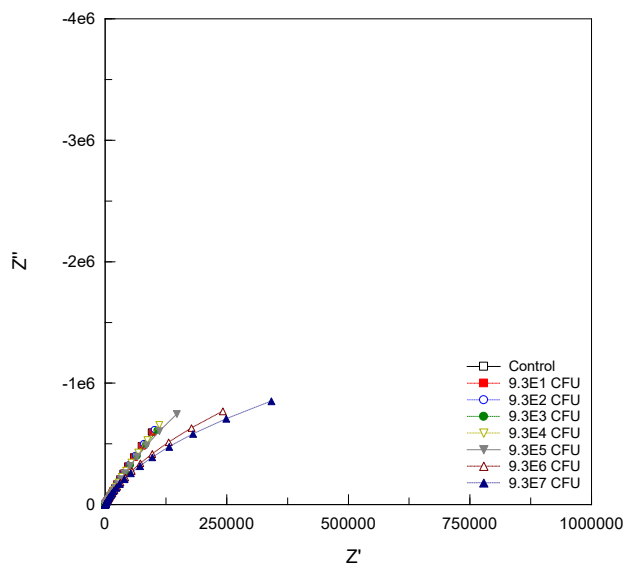
(c)

(d)

Figure 22. Nyquist diagram collected A) Gold IDE with 5μm gap size B) Gold IDE with 10μm gap size C) Platinum IDE with 5μm gap size D) Platinum IDE with 10μm gap size.

Results from the gold IDEs with a 5μm gap size seem to be divided into two groups: one below a concentration of 9.3 x10^4 CFU/ml, and one above. When the bacteria concentration reaches 9.3 x10^4 CFU/ml, the curves remain relatively stable until the maximum bacteria concentration was reached. This may be due to an increase and saturation of bacteria (planktonic and/or sessile) in contact with (or near) the IDE surface, filling the gaps between IDE electrodes. This would potentially result in a closed circuit between the interdigitated electrodes, triggering a more significant response. This increase in the impedance pattern could also be observed in the gold IDEs with 10 μm gap. In a similar manner, the bacteria concentration of 9.3x10^4 CFU/ml also seems a point that marks a divergence in pattern as it approaches the maximum concentration.

The impedance of the platinum IDEs shows an opposite trend to the gold IDEs with a decreasing impedance with increasing bacteria concentration. Furthermore, this drop is more noticeable than for the gold microchips. The platinum IDEs with the 5 μm gap seem to be slightly more sensitive as there is more differentiation in the slopes. It can also be seen that the response of the Z" values for the platinum 10 um group is roughly two times that of the platinum 5 um group, likely a result of the gap size is doubled.

The bode diagram (Figure 23) generally supports the observations found in the Nyquist diagram. The gold 10 μm group and the platinum 5 μm group both have noticeable changes in response when the bacteria concentration reaches a certain amount, while the gold 5 μm and platinum 10 μm groups have a converging pattern. Overall, the response (shape of the curves) for the gold IDEs with a 5 μm gap are somewhat distinct from the other three groups, suggesting that the EIS mechanism may be entirely different. In addition, the gold IDEs seem to have better sensitivity relative to the Platinum group.
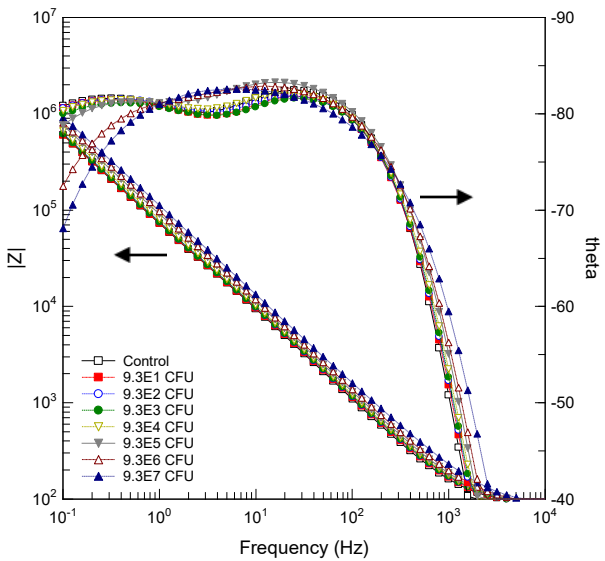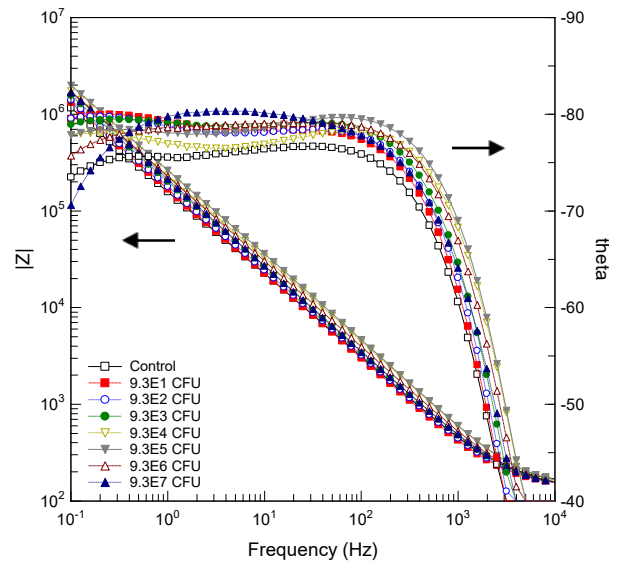
Figure 23. Bode diagram collected A) Gold IDE with 5µm gap size B) Gold IDE with 10µm gap size C) Platinum IDE with 5µm gap size D) Platinum IDE with 10µm gap size.
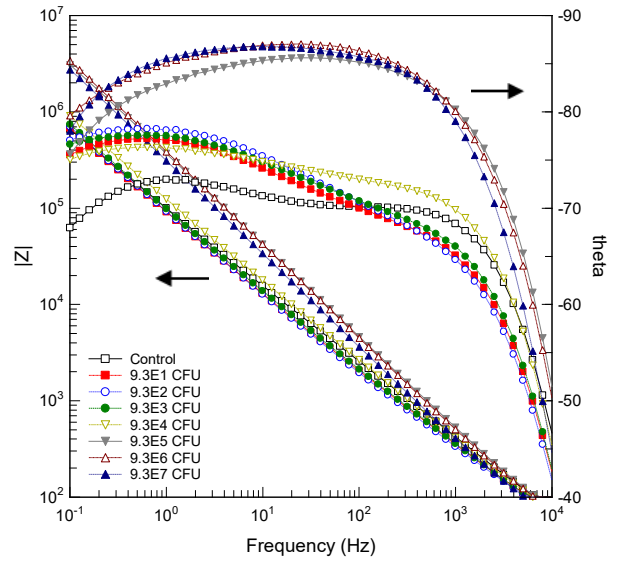
The reason for these noted differences in response between the gold and platinum IDEs is not entirely clear. That being said, this difference was consistently reproduced through repeated EIS scans and biological replicates.

4.2.2 Interpreting the EIS Data for IDE Testing (Total Bacteria Method)

An equivalent circuit for the IDE tests (total bacteria method) was selected based on the nature of the interface and was modified from Gonzalez et al [75]. A schematic of the circuit and its components is shown in Figure 24. This is effectively the same circuit used to interpret results for the parallel plate experiments reported earlier. The accuracy of the selected equivalent circuit was validated by determining the Chi^2 of the fitted model curve compared to the experimental results. The fitting process was performed using Gamry Echem Analyst Software. The equivalent circuit in Figure 24 had a $Chi^2 < 0.0004$ which is considered a good simulation. In this circuit, the CPE1 element acts effectively as a capacitor.

(a)   (b)
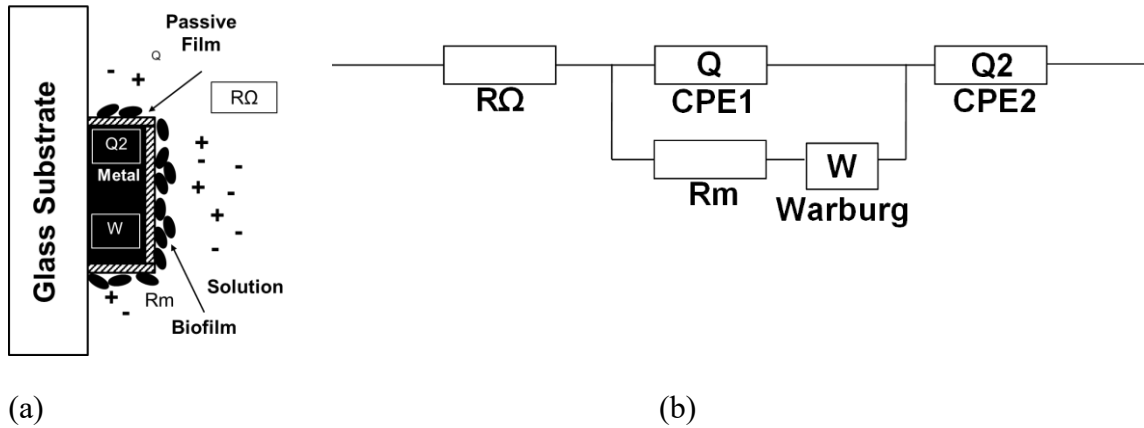
Figure 24. Equivalent circuit model used to evaluate the electrochemical response for the IDE sensor: (a) schematic of an IDE interface and (b) electric circuit elements (RΩ, Rm is the resistance of the solution, passive film respectively; CPE1 and CPE2 is the constant phase element of the passive film and metal, respectively; W is the "Warburg Element").

For the total bacteria test method, the effective capacitance of the IDEs as a function of the bacteria concentration is shown in Figure 25 for material type and each gap size combination. It can be seen that the gold IDEs with a 5 µm gap saw a significant change in effective capacitance at a bacteria concentration of approximately 10^4 CFU/ml. For all the other configurations (i.e. Au 10 µm, Pt 5 µm and Pt 10 µm), the effective capacitance response remains relatively stable for all bacteria concentrations with a slight decrease at around 10^5 CFU/ml. These results generally mimic those seen in the Nyquist diagram as a change of radius/slope for all groups were seen at approximately 10^5 CFU/ml.
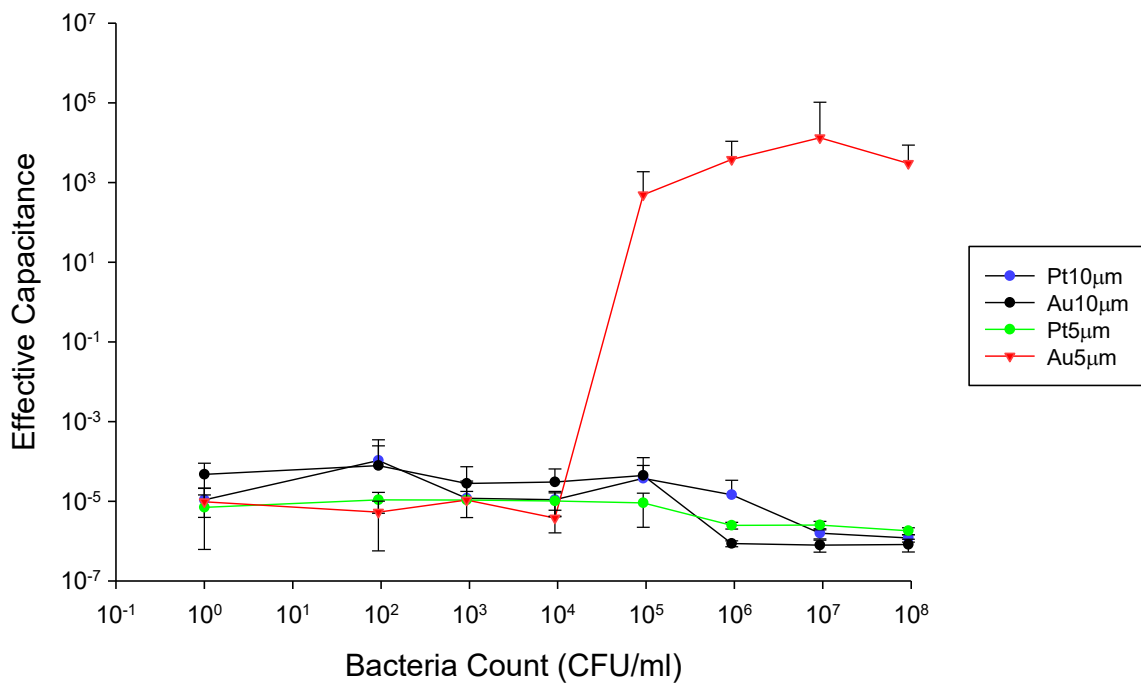
Figure 25. Change in Effective Capacitance with increasing bacteria concentration for various IDE configurations using the total bacteria method.

In addition to the effective capacitance (CPE1), the behaviour of the other elements of the model circuit was also examined. As shown in Figure 26, the resistance of the solution (RΩ) shows a more variable response with increasing bacteria concentration. In general, there is a relatively flat response up to a concentration of approximately 10^4 or 10^5 CFU/ml, at which point there is a slight increase in solution resistance for all microchips. Conversely, the resistance value of the passive film (Rm) stays relatively constant for all bacteria concentrations, as shown in Figure 27. The passive film resistance (Rm) for the platinum IDEs is greater than that for the gold IDEs which is not surprising since platinum is a less reactive metal than gold.

Based on these observed results, the effective capacitance seems to be the most sensitive to changes of bacteria concentration at the surface of the IDE, and may be the best approach to detect an aggregation of cell (i.e. such as the presence of a biofilm). However, this response was only seen for the gold IDEs with a 5 μm gap. As stated in the previous section, the spike in response at approximately 10^4 CFU/ml could be attributed to the aggregation of cells on or near the surface which creates a closed circuit between the microelectrode gaps (saturation effect). Based on this explanation, the sensitivity would then increase with decreasing gap size since bacteria cells are typically 1μm in length. This may also explain the lack of sensitivity for the gold IDEs with a 10 μm gap.

This effect is further demonstrated by optical microscope image taken of a gold IDE with as 5 μm gap, as shown in Figure 28. This image was taken immediately after the sample was withdrawn from the test solution, and shows the presence of bacteria on the surface. It can be seen that these cells are dense enough to connect one another between the electrodes, which may trigger the spike of the effective capacitance value. It should also be noted that the bacteria were quite active and moving relatively fast during observation.

In addition to the effective capacitance readings, the resistance of the solution ($R\Omega$) also shows some sensitivity with respect to bacteria concentration and may be an option to measure changes in microbial concentrations. Conversely, the resistance of the passive film (Rm) was seen to be effectively insensitive to bacteria concentration for all IDEs tested.

The observed results in measured effective capacitance and solution resistance can be further explained by examining the electric field profile for IDEs. Li et al. [81] and Wang et al. [82] modeled the electric field profiles for various IDE configurations. The field contour plots from their analyses are shown in Figure 29 and 30. It can be seen that the intensity of the electric field in the IDEs is greatest near the surface, and decreases significantly at distances away from the surface. In addition, there seems to be a spike in intensity at each edge of the flat IDE electrodes. These profiles clearly demonstrate that changes to capacitance and solution resistance will only be affected by the presence of bacteria directly on the surface or near the surface. As such, any local variation in bacteria cell concentration (e.g. localized agglomeration) may alter the observed electric field response which may explain the variation and scatter in the IDE results. This is in contrast to the parallel plate probe which theoretically has a more uniform electric field between the plates.
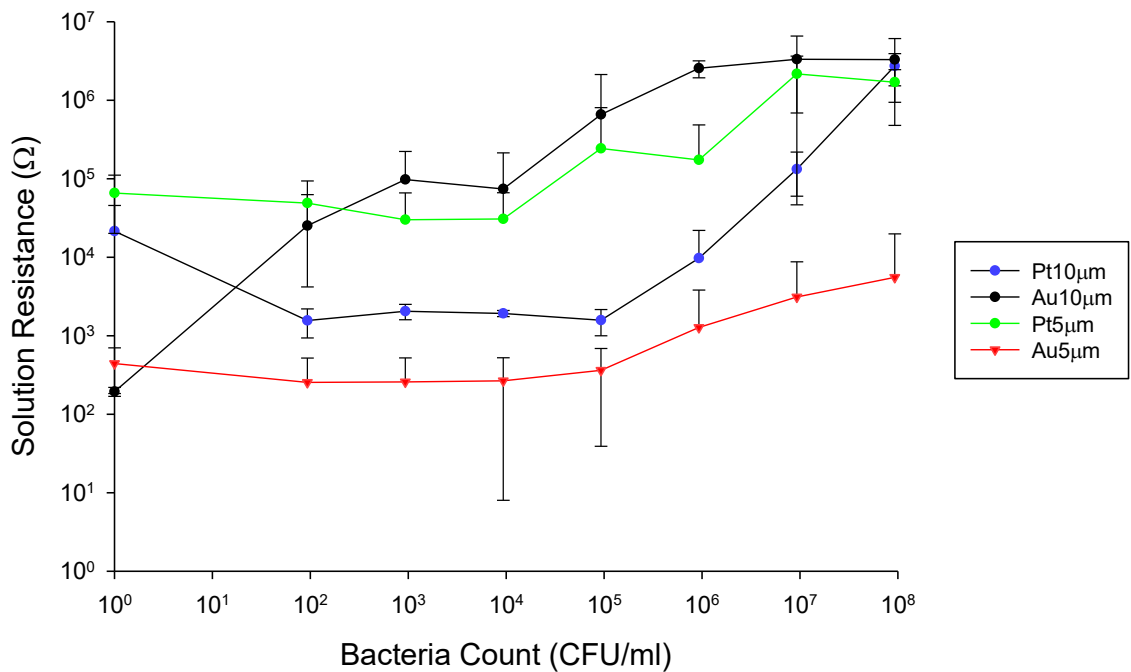
Figure 26. Change in Solution Resistance (RΩ) with increasing bacteria concentration for various IDE configurations using the total bacteria method.
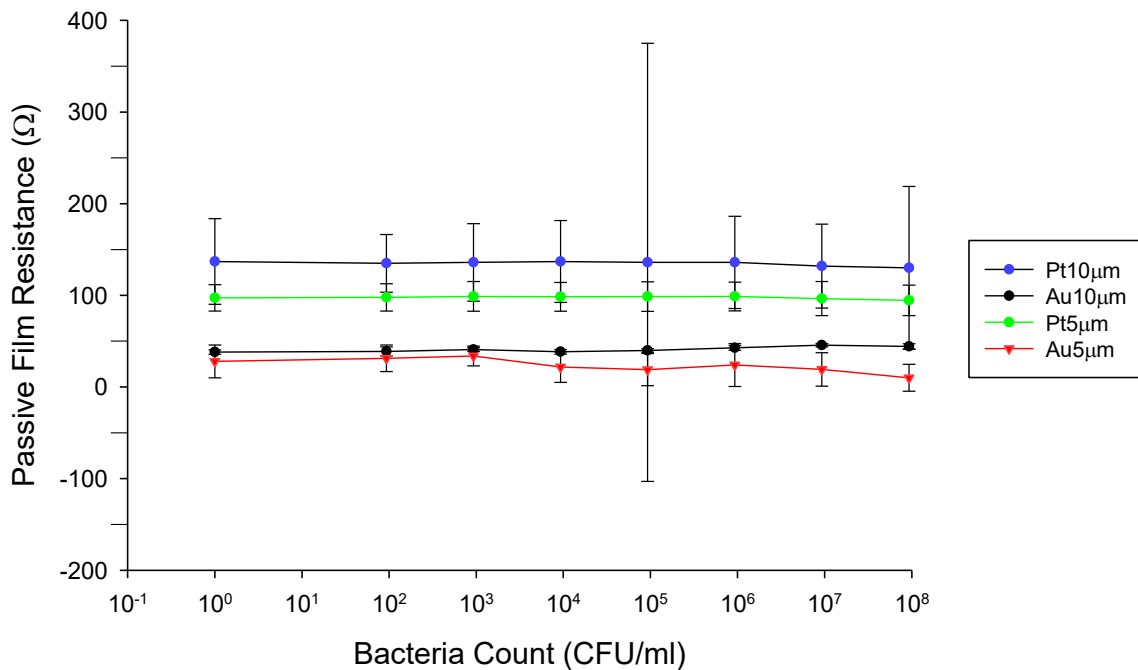
Figure 27. Change in Passive Film Resistance (Rm) with increasing bacteria concentration for various IDE configurations using the total bacteria method.
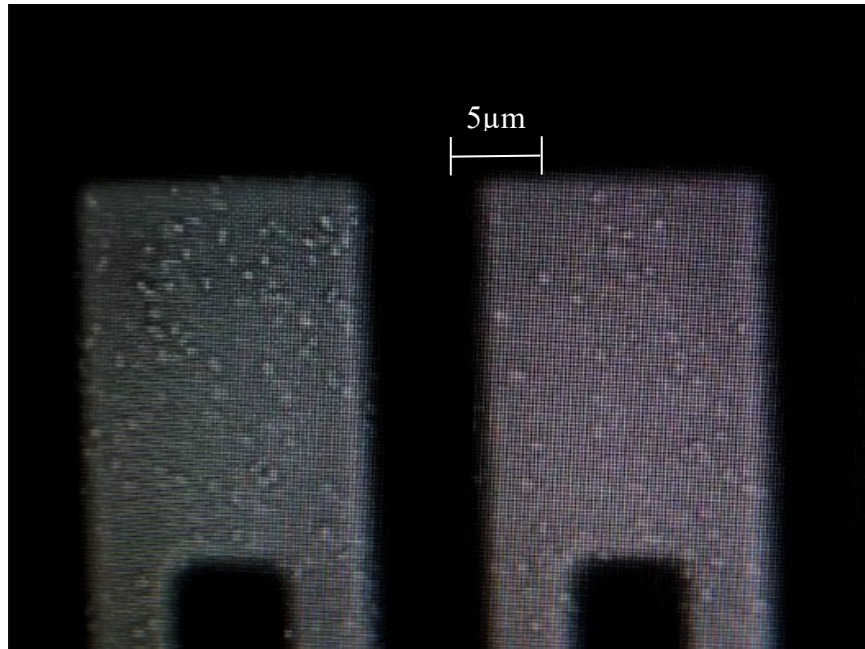
Figure 28. Microscopic image of Gold 5µm IDEs with bacteria cells (100X).
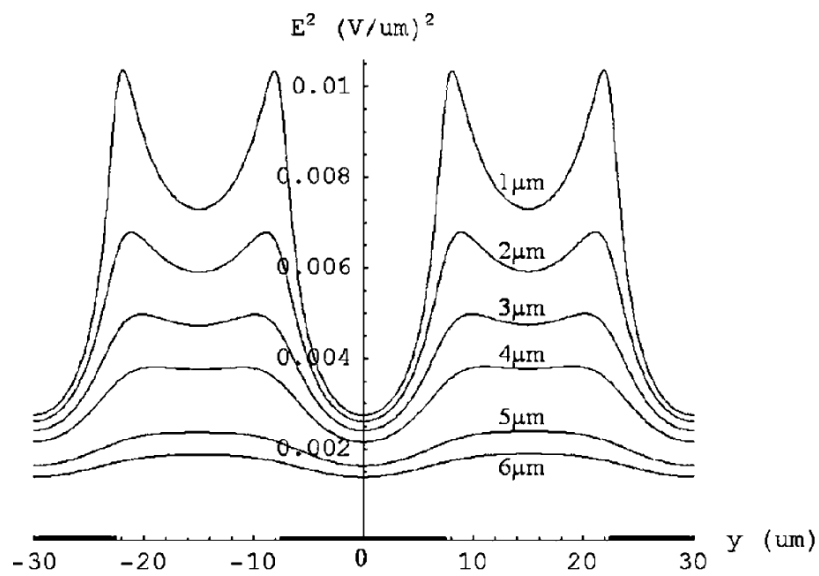
Figure 29. Simulated electric field parameter from the different heights above the IDE with a length of 15 µm[81][9].
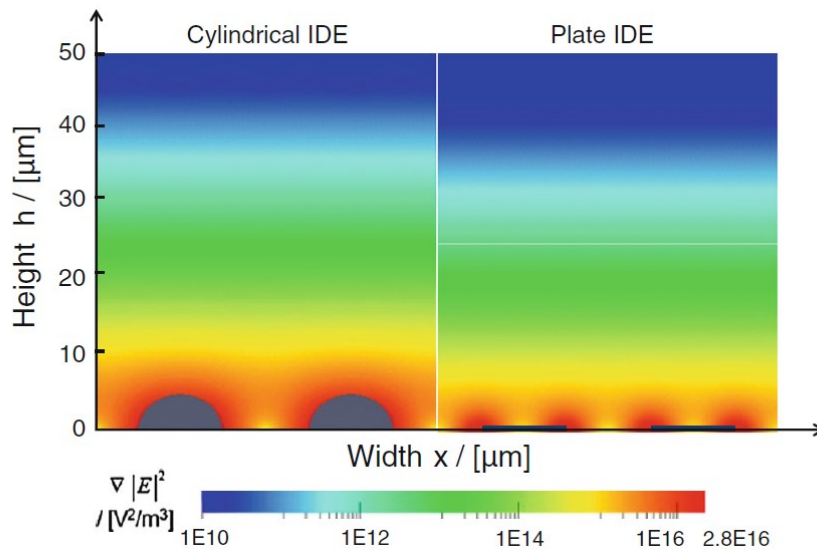
Figure 30. Simulation of electric field gradient squared for cylindrical IDE (left) and plate IDE (right)[82] [10].

4.3 IDE Test Results (Sessile Bacteria Method)

EIS measurements of the IDEs tested using the sessile bacteria method (i.e. exposing the IDE directly to a growing culture) is presented in this section. Basic EIS response curves (Nyquist and Bode diagrams) were excluded for brevity. The base EIS data was fit to the same equivalent circuit used for the IDE total bacteria tests in the previous section (see Figure 24). The accuracy of the equivalent circuit for the sessile method was again validated using the Chi^2 fit of the model to the experimental data points and was found to be a good simulation ($Chi^2 < 0.0004$).

The effective capacitance of the IDE (sessile bacteria testing) as a function of the bacteria concentration is shown in Figure 31 for each gap size and materials combination. Overall, it can be seen that the effective capacitance for all combinations slightly decreases from their control

---

[10] Figure reproduced with permission.

conditions (0 CFU/ml), but there is no clear trend for any of the combinations tested due to clustering of data points and significant scatter of the readings. In addition to the effective capacitance (CPE1), responses of other elements in the model circuit were also examined, as shown in Figure 32 and 33. Again, there seems to be no clear trend for any of the IDE combinations tested.

It should be noted that the bacteria concentration for this sessile bacteria method was difficult to control over time as seen by the clustering of concentration values taken over the four-day sampling period. This is in contrast to the total bacteria methodology highlighted in the previous sections where bacteria concentrations were well controlled. This suggests that improvements to the sessile method will need to be made if this method is to be used for validating IDEs in the future.
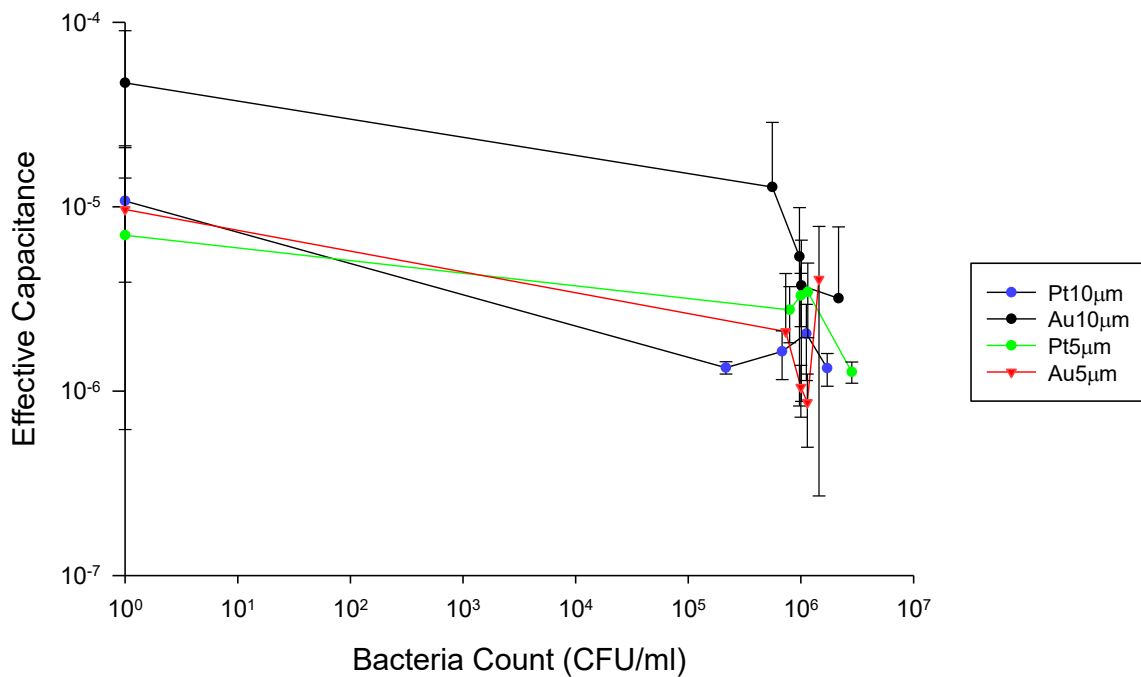
Figure 31. Change in Effective Capacitance with increasing bacteria concentration for various IDE configurations using the sessile bacteria method.
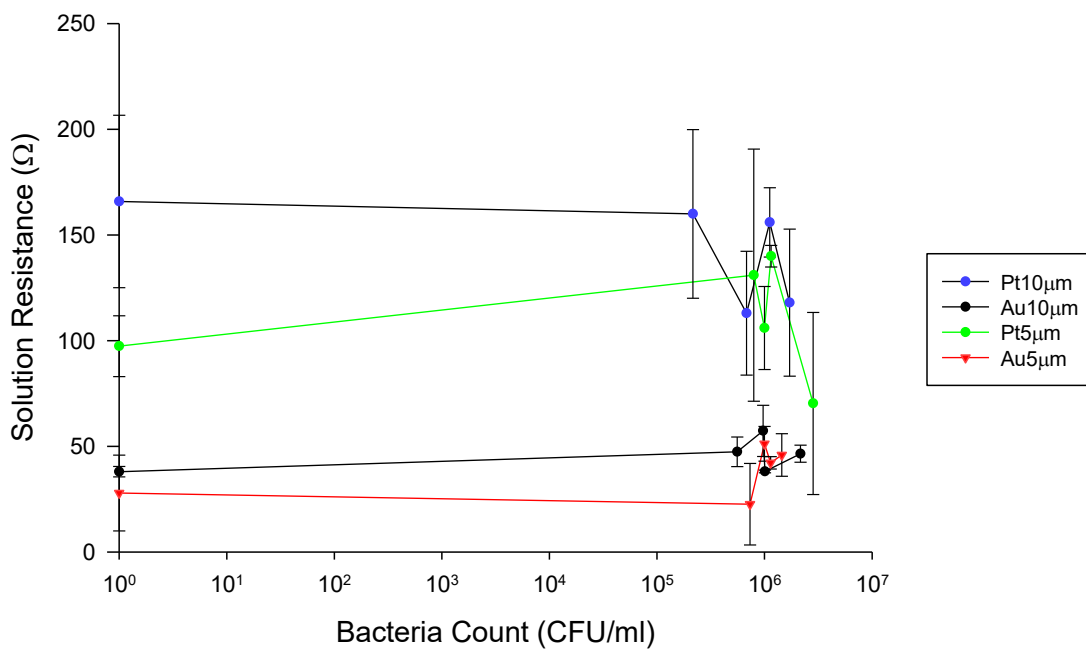

Figure 32. Change in Solution Resistance (RΩ) with increasing bacteria concentration for various IDE configurations using the sessile bacteria method.
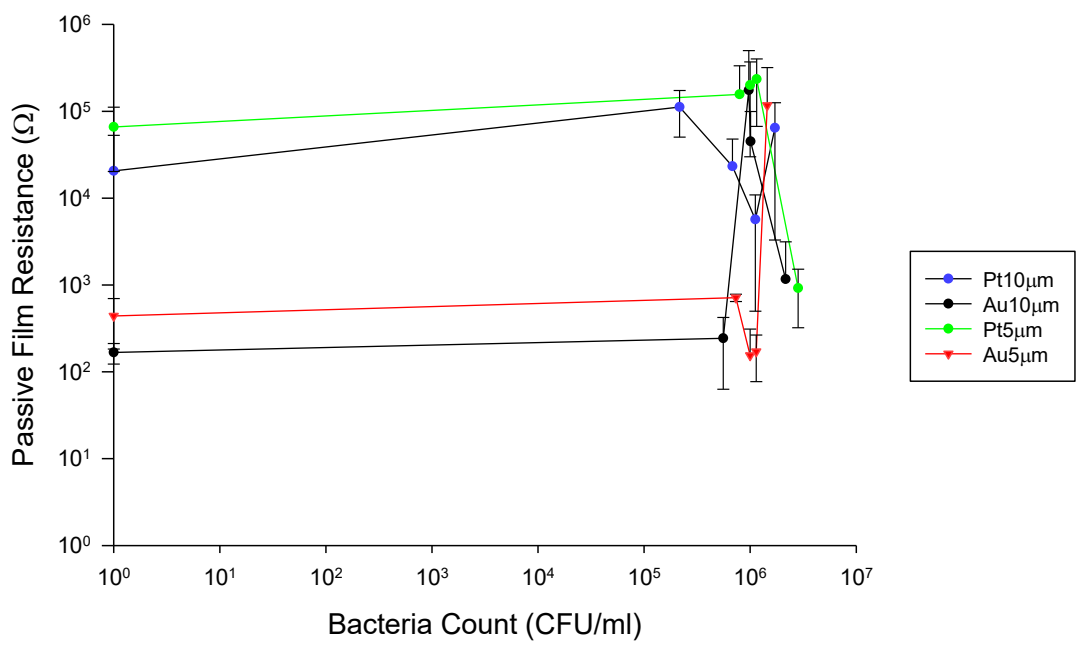
Figure 33. Change in Passive Film Resistance (Rm) with increasing bacteria concentration for various IDE configurations using the sessile bacteria method.

5. CONCLUSIONS

This study has described the assessment of two probe systems for detecting the presence of bacteria using electrochemical methods: a) parallel plate probes, and b) interdigitated electrode (IDE) microchips. Measurements were made using Electrochemical Impedance Spectroscopy (EIS) in an attempt to correlate bacteria concentration with common electrochemical parameters such as impedance and capacitance. Two different methodologies were developed to assess whether these probes can effectively detect and measure specific quantities of microorganisms in a fluid system: a). the "total bacteria method" which measures both planktonic and sessile bacteria by immersing the probe in a fluid bath with a known (fixed) bacteria concentration, and b). the "sessile bacteria method" which measures the concentration of bacteria deposited on the probe surface when it is immersed in a growing culture. The first method (total bacteria method) was used to evaluate both the parallel plate and IDE microchips, while the second method (sessile bacteria method) was only used for the IDE microchips.

In terms of findings, basic results from the EIS spectrum (Nyquist and Bode plots) were able to discern changes in bacteria concentration for both the parallel plate setup and certain IDE tests. However, these basic EIS datasets were found to be too complex for analyzing target bacteria thresholds for detection in practice. In order to improve the utility of (and simplify) the EIS data, an equivalent electrical circuit model was successfully selected to better reflect the nature of the interface under study for both the parallel plate setup and the IDE setup. From this circuit, the equivalent capacitance of the passive film was determined using a constant phase element, and other circuit parameters, such as solution and passive resistances, were also assessed.

For the parallel plate system, the effective capacitance parameter was shown to be an effective parameter to detect and quantify increasing bacteria concentrations. For the various parallel plate probe configurations tested, the threshold of detection all occurred at a bacteria concentration of approximately 10^8 CFU/ml. A similar trend was also seen for the gold IDE microchips (5 µm gap) using the total bacteria test method. The threshold of detection for this probe occurred at a bacteria concentration of approximately 10^4 CFU/ml. These thresholds likely represent the aggregation of the cells at or near the surfaces of the probes which effectively creates a closed circuit. The solution resistance for all the IDEs tested using the total bacteria method was also seen to gradually increase with increasing bacteria concentration, however, the threshold was not as distinct as for the effective capacitance parameter.

There was a general lack of consistency for a number of the IDE microchip configurations tested (including the gold IDE with a 10 µm gap and the platinum IDEs with a 5 and 10 µm gap). It is speculated that the 10 µm gap may not be sensitive enough to detect the microorganisms used in the study due to the size of the bacteria, and due to the decrease in electric field potential at wider gaps.

In terms of test methodologies examined, the total bacteria test methodology was found to produce consistent results for increasing bacteria concentrations. The sessile test methodology, however, was not as successful due to difficulties in controlling bacteria concentrations over time (resulting in clustering of data). This made it extremely difficult to assess the resulting changes to the measured electrochemical parameters.

Overall, this "proof of concept" study demonstrates the potential for viable, real-time detection methods for systems susceptible to biofouling and/or MIC. However, further work is necessary to make these approaches more practical.

6. FUTURE WORK

While this study has demonstrated a novel approach to detecting and quantifying bacteria concentrations in fluid systems, there is further research and development required to better understand the phenomena observed, and to better improve the experimental methods for system validation. Suggestions on future studies based on this thesis are as follows:

1). Optimization of the parallel plate probe — The parallel plate design could be further optimized to reduce the size of the probe, and to modify the clamping system to allow for easier disassembly and improved exposure to the fluid system. Additionally, other materials and probe designs could be explored to optimize the testing performance and sensitivity of the system.

2). Testing of systems with MIC related microorganisms – If these types of probes are to be used to detect MIC related systems, more representative microbiological strains will need to be tested (e.g. anaerobic strains, gram-positive strains). Furthermore, it also would be beneficial to test these probes with more representative communities (mixed culture), and with produced fluids/sludges taken directly from actual water systems or oil & gas pipelines. Column chromatography could be applied to study the effect of metabolism products on the test probes.

3). Characterization of bacteria behavior using advanced microscopy – Further extension of this research should include the use of advanced microscopy techniques to better understand the behavior of the bacteria either ex-situ (microscopic characterization immediately after testing), or in-situ (modify the test apparatus to visualize bacteria interaction with the two probe designs). The latter approach would be particularly useful in better understanding the effects of materials, gap sizes, and applied EIS signals, and to possibly correlate observed microbial counts with other quantification methods.

References

[1] National Commission on Energy Policy (US). Ending the energy stalemate: A bipartisan strategy to meet America's energy challenges. National Commission on Energy Policy, 2004.

[2] Kraemer, Daniel, et al. "Solar assisted method for recovery of bitumen from oil sand." *Applied Energy* 86.9 (2009): 1437-1441.

[3] "Energy Transition Outlook 2017." Energy Transition Outlook | DNV GL, DNV GL, 2017, eto.dnvgl.com/2017.

[4] Canada, Natural Resources. "Government of Canada / Gouvernement Du Canada." Natural Resources Canada, Government of Canada / Gouvernement Du Canada, 25 July 2016, www.nrcan.gc.ca/our-natural-resources/energy-sources-distribution/clean-fossil-fuels/pipelines/pipelines-across-canada/18856.

[5] Crone, T. J., & Tolstoy, M. (2010). Magnitude of the 2010 Gulf of Mexico oil leak. *Science*, *330*(6004), 634-634.

[6] NACE IMPACT Study, 2016. impact.nace.org (Accessed 1 September 2019).

[7] Van Hamme, J. D., Singh, A., & Ward, O. P. (2003). Recent advances in petroleum microbiology. *Microbiology and molecular biology reviews*, *67*(4), 503-549.

[8] Eckert, R. B., & Skovhus, T. L. (2018). Advances in the application of molecular microbiological methods in the oil and gas industry and links to microbiologically influenced corrosion. *International Biodeterioration & Biodegradation*, *126*, 169-176.

[9] Tamachkiarow, A., & Flemming, H. C. (2003). On-line monitoring of biofilm formation in a brewery water pipeline system with a fibre optical device. *Water Science and Technology*, *47*(5), 19-24.

[10] Kujundzic, E., Cobry, K., Greenberg, A. R., & Hernandez, M. (2008). Use of ultrasonic sensors for characterization of membrane fouling and cleaning. *Journal of Engineered Fibers and Fabrics*, *3*(2), 155892500800300211.

[11] Zabriskie, D. W., & Humphrey, A. E. (1978). Estimation of fermentation biomass concentration by measuring culture fluorescence. *Applied and environmental microbiology*, *35*(2), 337-343.

[12] Dixon, M. C. (2008). Quartz crystal microbalance with dissipation monitoring: enabling real-time characterization of biological materials and their interactions. *Journal of biomolecular techniques: JBT*, *19*(3), 151.

[13] Nivens, D. E., Chambers, J. Q., Anderson, T. R., Tunlid, A., Smit, J., & White, D. C. (1993). Monitoring microbiol adhesion and biofilm formation by attenuated total reflection/Fourier transform infrared spectroscopy. *Journal of microbiological methods*, *17*(3), 199-213.

[14] Renslow, R. S., Majors, P. D., McLean, J. S., Fredrickson, J. K., Ahmed, B., & Beyenal, H. (2010). In situ effective diffusion coefficient profiles in live biofilms using pulsed-field gradient nuclear magnetic resonance. *Biotechnology and Bioengineering*, *106*(6), 928-937.

[15] Mollica, A., & Cristiani, P. (2003). On-line biofilm monitoring by" BIOX" electrochemical probe. *Water Science and Technology*, *47*(5), 45-49.

[16] Franklin, M. J., Nivens, D. E., Guckert, J. B., & White, D. C. (1991). Effect of electrochemical impedance spectroscopy on microbial biofilm cell numbers, viability, and activity. *Corrosion*, *47*(7), 519-522.

[17] Janknecht, P., & Melo, L. F. (2003). Online biofilm monitoring. *Reviews in Environmental Science and Biotechnology*, *2*(2-4), 269-283.

[18] Ibrahim, T. H., Gomes, E. E., Obot, I. B., Khamis, M., & Sabri, M. A. (2017). Mild steel green inhibition by Ficus carica leaves extract under practical field conditions. *Journal of adhesion science and Technology*, *31*(24), 2697-2718.

[19] Little, B. J., & Lee, J. S. (2007). *Microbiologically influenced corrosion* (Vol. 3). John Wiley & Sons.

[20] Little, B., Wagner, P., & Mansfeld, F. (1992). An overview of microbiologically influenced corrosion. *Electrochimica acta*, *37*(12), 2185-2194.

[21] Borenstein, S. (1994). *Microbiologically influenced corrosion handbook*. Elsevier.

[22] Kip, N., & Van Veen, J. A. (2015). The dual role of microbes in corrosion. *The ISME journal*, *9*(3), 542-551.

[23] Enning, D., & Garrelfs, J. (2014). Corrosion of iron by sulfate-reducing bacteria: new views of an old problem. *Applied and environmental microbiology*, *80*(4), 1226-1236.

[24] Skovhus, T. L., Enning, D., & Lee, J. S. (2017). Microbiologically Influenced Corrosion in the Upstream Oil and Gas Industry. CRC Press.

[25] Jefferson, K. K. (2004). What drives bacteria to produce a biofilm? *FEMS microbiology letters*, 236(2), 163-173.

[26] Characklis, W. G. (1981). Bioengineering report: fouling biofilm development: a process analysis. *Biotechnology and Bioengineering*, 23(9), 1923-1960.

[27] Sauer, K., Camper, A. K., Ehrlich, G. D., Costerton, J. W., & Davies, D. G. (2002). Pseudomonas aeruginosa displays multiple phenotypes during development as a biofilm. *Journal of bacteriology*, 184(4), 1140-1154.

[28] Daniels, R., Vanderleyden, J., & Michiels, J. (2004). Quorum sensing and swarming migration in bacteria. *FEMS microbiology reviews*, 28(3), 261-289.

[29] Eckert, R. B., & Skovhus, T. L. (2018). Advances in the application of molecular microbiological methods in the oil and gas industry and links to microbiologically influenced corrosion. *International Biodeterioration & Biodegradation*, *126*, 169-176.

[30] Arrage, A. A., Vasishtha, N., Sundberg, D., Bausch, G., Vincent, H. L., & White, D. C. (1995). On-line monitoring of antifouling and fouling-release surfaces using bioluminescence and fluorescence measurements during laminar flow. *Journal of industrial microbiology*, *15*(4), 277-282.

[31] Wolf, G., Almeida, J. S., Crespo, J. G., & Reis, M. A. M. (2003). Monitoring of biofilm reactors using natural fluorescence fingerprints. *Water Science and Technology*, 47(5), 161.

[32] Duysens, L. N. M., & Amesz, J. (1957). Fluorescence spectrophotometry of reduced phosphopyridine nucleotide in intact cells in the near-ultraviolet and visible region. *Biochimica et biophysica acta*, *24*, 19-26.

[33] Quilès, F., Saadi, S., Francius, G., Bacharouche, J., & Humbert, F. (2016). In situ and real time investigation of the evolution of a Pseudomonas fluorescens nascent biofilm in the presence of an antimicrobial peptide. *Biochimica et Biophysica Acta (BBA)-Biomembranes*, *1858*(1), 75-84.

[34] Bell, A. G. (1881). On the production and reproduction of sound by light. In *Proc. Am. Assoc. Adv. Sci.* (Vol. 29, pp. 115-136).

[35] Miklós, A., Schäfer, S., & Hess, P. (1999). Electronic spectroscopy/vibrational, rotational & raman spectroscopies. *Photoacoustic spectroscopy, theory, 1815-1822.*

[36] Rosencwaig, A., & Gersho, A. (1975). Theory of the photoacoustic effect with solids. *The Journal of the Acoustical Society of America*, *58*(S1), S52-S52.

[37] Tam, A. C. (1986). Applications of photoacoustic sensing techniques. *Reviews of Modern Physics*, *58*(2), 381.

[38] Karabutov, A. A., Podymova, N. B., & Letokhov, V. S. (1995). Time-resolved optoacoustic measurement of absorption of light by inhomogeneous media. *Applied optics*, *34*(9), 1484-1487.

[39] Schmid, T., Panne, U., Haisch, C., & Niessner, R. (2003). Biofilm monitoring by photoacoustic spectroscopy. *Water Science and Technology*, *47*(5), 25-29.

[40] Pang, P., Xiao, X., Cai, Q., Yao, S., & Grimes, C. A. (2008). A wireless magnetoelastic-sensing device for in situ evaluation of Pseudomonas aeruginosa biofilm formation. *Sensors and Actuators B: Chemical*, *133*(2), 473-477.

[41] Grimes, C., Mungle, C., Zeng, K., Jain, M., Dreschel, W., Paulose, M., & Ong, K. (2002). Wireless magnetoelastic resonance sensors: A critical review. *Sensors*, *2*(7), 294-313.

[42] Grimes, C. A., Roy, S. C., Rani, S., & Cai, Q. (2011). Theory, instrumentation and applications of magnetoelastic resonance sensors: a review. *Sensors*, *11*(3), 2809-2844.

[43] Lakshmanan, R. S., Guntupalli, R., Hu, J., Kim, D. J., Petrenko, V. A., Barbaree, J. M., & Chin, B. A. (2007). Phage immobilized magnetoelastic sensor for the detection of Salmonella typhimurium. *Journal of microbiological methods*, *71*(1), 55-60.

[44] Ong, K. G., Zeng, K., Yang, X., Shankar, K., Ruan, C., & Grimes, C. A. (2006). Quantification of multiple bioagents with wireless, remote-query magnetoelastic microsensors. *IEEE Sensors Journal*, *6*(3), 514-523.

[45] Kujundzic, E., Fonseca, A. C., Evans, E. A., Peterson, M., Greenberg, A. R., & Hernandez, M. (2007). Ultrasonic monitoring of earlystage biofilm growth on polymeric surfaces. *Journal of microbiological methods*, *68*(3), 458-467.

[46] Ramaswamy, S., Greenberg, A. R., & Peterson, M. L. (2004). Non-invasive measurement of membrane morphology via UFDR: pore-size characterization. *Journal of membrane science*, *239*(1), 143-154.

[47] Krantz, W. B., & Greenberg, A. R. (2008). Membrane Characterization by Ultrasonic Time-Domain Reflectometry. *Advanced Membrane Technology and Applications*, 879-897.

[48] Sim, S. T. V., Suwarno, S. R., Chong, T. H., Krantz, W. B., & Fane, A. G. (2013). Monitoring membrane biofouling via ultrasonic time-domain reflectometry enhanced by silica dosing. *Journal of membrane science*, *428*, 24-37.

[49] Hou, Y. L., Li, J. X., Gao, Y. N., Xu, X. C., Cai, Y., & Yang, N. (2010). Monitoring of CaSO4 deposition behaviors on biofilm during nanofiltration via ultrasonic time-domain reflectometry (UTDR). *Water Science and Technology*, *61*(11), 2853-2861.

[50] G. Sauerbrey Z. Phys., 155 (1955), p. 206

[51] Schofield, A. L., Rudd, T. R., Martin, D. S., Fernig, D. G., & Edwards, C. (2007). Real-time monitoring of the development and stability of biofilms of Streptococcus mutans using the quartz crystal microbalance with dissipation monitoring. *Biosensors and Bioelectronics*, *23*(3), 407-413.

[52] Nivens, D. E., Chambers, J. Q., Anderson, T. R., & White, D. C. (1993). Long-term, on-line monitoring of microbial biofilms using a quartz crystal microbalance. *Analytical Chemistry*, *65*(1), 65-69.

[53] Fercher, A. F., Drexler, W., Hitzenberger, C. K., & Lasser, T. (2003). Optical coherence tomography-principles and applications. *Reports on progress in physics*, *66*(2), 239.

[54] Haisch, C., & Niessner, R. (2007). Visualisation of transient processes in biofilms by optical coherence tomography. *Water research*, *41*(11), 2467-2472.

[55] Fortunato, L., & Leiknes, T. (2017). In-situ biofouling assessment in spacer filled channels using optical coherence tomography (OCT): 3D biofilm thickness mapping. *Bioresource technology*, *229*, 231-235.

[56] Suci, P. A., Siedlecki, K. J., Palmer, R. J., White, D. C., & Geesey, G. G. (1997). Combined light microscopy and attenuated total reflection fourier transform infrared spectroscopy for integration of biofilm structure, distribution, and chemistry at solid-liquid interfaces. *Applied and environmental microbiology*, *63*(11), 4600-4603.

[57] Quilès, F., Humbert, F., & Delille, A. (2010). Analysis of changes in attenuated total reflection FTIR fingerprints of Pseudomonas fluorescens from planktonic state to nascent biofilm state. *Spectrochimica Acta Part A: Molecular and Biomolecular Spectroscopy*, *75*(2), 610-616.

[58] Meyer, M. T., Roy, V., Bentley, W. E., & Ghodssi, R. (2011). Development and validation of a microfluidic reactor for biofilm monitoring via optical methods. *Journal of Micromechanics and Microengineering*, *21*(5), 054023.

[59] Suehiro, J., Yatsunami, R., Hamada, R., & Hara, M. (1999). Quantitative estimation of biological cell concentration suspended in aqueous medium by using dielectrophoretic impedance measurement method. *Journal of Physics D: Applied Physics*, *32*(21), 2814.

[60] Yerly, J., Hu, Y., Jones, S. M., & Martinuzzi, R. J. (2007). A two-step procedure for automatic and accurate segmentation of volumetric CLSM biofilm images. *Journal of microbiological methods*, *70*(3), 424-433

[61] Shanks, J. V. (2001). In situ NMR systems. *Current issues in molecular biology*, *3*(1), 15.

[62] Majors, P. D., McLean, J. S., Pinchuk, G. E., Fredrickson, J. K., Gorby, Y. A., Minard, K. R., & Wind, R. A. (2005). NMR methods for in situ biofilm metabolism studies. *Journal of microbiological methods*, 62(3), 337-344.

[63] Renslow, R. S., Majors, P. D., McLean, J. S., Fredrickson, J. K., Ahmed, B., & Beyenal, H. (2010). In situ effective diffusion coefficient profiles in live biofilms using pulsed-field gradient nuclear magnetic resonance. *Biotechnology and bioengineering*, *106*(6), 928-937.

[64] Renslow, R. S., Babauta, J. T., Dohnalkova, A. C., Boyanov, M. I., Kemner, K. M., Majors, P. D., ... & Beyenal, H. (2013). Metabolic spatial variability in electrode-respiring Geobacter sulfurreducens biofilms. *Energy & environmental science*, *6*(6), 1827-1836.

[65] Marsili, E., Rollefson, J. B., Baron, D. B., Hozalski, R. M., & Bond, D. R. (2008). Microbial biofilm voltammetry: direct electrochemical characterization of catalytic electrode-attached biofilms. *Applied and environmental microbiology*, *74*(23), 7329-7337.

[66] Pavanello, G., Faimali, M., Pittore, M., Mollica, A., Mollica, A., & Mollica, A. (2011). Exploiting a new electrochemical sensor for biofilm monitoring and water treatment optimization. *Water research*, *45*(4), 1651-1658.

[67] Hsu, C. I., Wang, G. L., Ger, M. D., & Hou, K. H. (2016). Corrosion behaviour of electroless deposited Ni–P/BN (h) composite coating. *Int. J. Electrochem. Sci*, *11*, 4352-4361.

[68] Yadav, D. K., Chauhan, D. S., Ahamad, I., & Quraishi, M. A. (2013). Electrochemical behavior of steel/acid interface: adsorption and inhibition effect of oligomeric aniline. *RSC advances*, *3*(2), 632-646.

[69] Hause, Lawrence L., Richard A. Komorowski, and Francis Gayon. "Electrode and electrolyte impedance in the detection of bacterial growth." *IEEE Transactions on Biomedical Engineering* 5 (1981): 403-410.

[70] Fehrenbach, R., Comberbach, M., & Petre, J. O. (1992). On-line biomass monitoring by capacitance measurement. *Journal of biotechnology*, *23*(3), 303-314.

[71] Franco, R., C. D. Bortner, and J. A. Cidlowski. "Potential roles of electrogenic ion transport and plasma membrane depolarization in apoptosis." *The Journal of membrane biology* 209.1 (2006): 43-58

[72] Lvovich, V. (2014). *"AC Impedance Spectroscopy Measurement - Understanding the Effects of 2-, 3-, and 4-Electrode Cells and Cables on Experimental Data"*. Norwich, N.Y.: Knovel.

[73] Duan, J., Wu, S., Zhang, X., Huang, G., Du, M., & Hou, B. (2008). Corrosion of carbon steel influenced by anaerobic biofilm in natural seawater. *Electrochimica Acta*, *54*(1), 22-28.

[74] Gonzalez, J. E. G., Santana, A. F., & Mirza-Rosca, J. C. (1998). Effect of bacterial biofilm on 316 SS corrosion in natural seawater by EIS. *Corrosion science*, *40*(12), 2141-2154.

[75] Castaneda, H., & Benetton, X. D. (2008). SRB-biofilm influence in active corrosion sites formed at the steel-electrolyte interface when exposed to artificial seawater conditions. *Corrosion Science*, *50*(4), 1169-1183.

[76] Obuekwe, C. O., Westlake, D. W. S., & Plambeck, J. A. (1987). Evidence that available energy is a limiting factor in the bacterial corrosion of mild steel by a Pseudomonas sp. *Canadian journal of microbiology*, 33(3), 272-275.

[77] Auerbach, I. D., Sorensen, C., Hansma, H. G., & Holden, P. A. (2000). Physical morphology and surface properties of unsaturated Pseudomonas putida biofilms. *Journal of bacteriology*, 182(13), 3809-3815.

[78] Wallace, W. H., Rice, J. F., White, D. C., & Sayler, G. S. (1994). Distribution of alginate genes in bacterial isolates from corroded metal surfaces. *Microbial ecology*, 27(3), 213-223.

[79] Dubey, R. S., T. K. G. Namboodhiri, and S. N. Upadhyay. "Microbiologically influenced corrosion of mild steel of cultures of sulphate reducing bacteria." (1995).

[80] Feng, K., Wu, G., Li, Z., Cai, X., & Chu, P. K. (2011). Corrosion behavior of SS316L in simulated and accelerated PEMFC environments. *international journal of hydrogen energy*, *36*(20), 13032-13042.

[81] Li, H., & Bashir, R. (2002). Dielectrophoretic separation and manipulation of live and heat-treated cells of Listeria on microfabricated devices with interdigitated electrodes. *Sensors and actuators B: chemical*, *86*(2-3), 215-221.

[82] Wang, Y., Du, F., Baune, M., & Thöming, J. (2014). Dielectrophoresis in aqueous suspension: impact of electrode configuration. Microfluidics and nanofluidics, 17(3), 499-507.